EVALUATING PLUTON-VOLCANO RELATIONSHIPS: AN EXAMPLE FROM THE MOUNT GIVENS GRANODIORITE

Ryan E. Frazer

A thesis submitted to the faculty of the University of North Carolina at Chapel Hill in partial fulfillment of the requirements for the degree of Master of Science in the Department of Geological Sciences.

Chapel Hill
2013

Approved by:

Drew S. Coleman

Allen F. Glazner

Kevin G. Stewart

ABSTRACT

RYAN E. FRAZER: Evaluating pluton-volcano relationships:
an example from the Mount Givens Granodiorite
(Under the direction of Drew S. Coleman)

Zircon U-Pb geochronology indicates that the Mount Givens Granodiorite (MGG) of the Sierra Nevada batholith, California, was constructed over at least 7 Ma from 98-91 Ma. Chemical and volumetric similarities between homogenous ignimbrites (monotonous intermediates; MIs) and plutons such as the MGG led some to suggest a genetic relationship between the two. However, there are three issues regarding this link: 1) large plutons like the MGG accumulated at estimated rates of 0.001 km^3/a, 1-2 orders of magnitude less than fluxes calculated for MIs; 2) zircon dissolution modeling indicates that rejuvenation events thought to affect MIs would not sufficiently dissolve zircon that should record multi-Ma growth of a crystal-rich mush 3) the Sierra Nevada batholith apparently lacks mafic plutons large enough to initiate MI eruptions. I suggest that MI eruptions are caused by high flux events, leaving little behind in the intrusive rock record, whereas low fluxes favor pluton growth.

ACKNOWLEDGEMENTS

I would foremost like to thank my advisor, Dr. Drew S. Coleman, for his vision, direction, encouragement and humor, which were fundamental to the successful completion of this project. I would also like to thank Dr. Allen F. Glazner for his valuable knowledge and comments on the project, and Dr. Kevin S. Stewart for his insights and support.

This project benefitted greatly from conversations and technical aid from Drs. Ryan D. Mills and Jeremy Inglis. I would also like to acknowledge Miquela Ingalls for lending assistance in the lab and Courtney Beck for her cheerful help in the field. The support of my family and especially Sarah Miller were essential my work on this project. I would like to acknowledge Sigma Xi, the Geological Society of America and especially the Martin Fund of the University of North Carolina at Chapel Hill Geological Sciences Department for financially supporting this project.

TABLE OF CONTENTS

LIST OF TABLES

Table

LIST OF FIGURES

Figure

LIST OF ABBREVIATIONS

a	annum
AMS	anisotropy of magnetic susceptibility
ka	thousands of years/thousands of years before present
Ma	millions of years/millions of years before present
MGG	Mount Givens Granodiorite
MI	monotonous intermediate
TIMS	thermal ionization mass spectrometer
T	temperature
t	time

I. INTRODUCTION

Understanding the relationships between intrusive and extrusive magmatic rocks is a fundamental problem in igneous petrology. Some large plutons and zoned intrusive suites have been interpreted to either be unerupted crystal mushes or the crystalline residues left behind after large ignimbrite eruptions (Hamilton and Myers 1967; Hildreth 2004; Bachmann et al. 2007; Lipman 2007). In this hypothesis, both plutons and ignimbrites share the same histories as they are constructed incrementally as crystal-rich mushes over hundreds of thousands to millions of years. With no further inputs of magma, the mush may cool to form a granodiorite pluton. Conversely, the mush may be rejuvenated by energy inputs, including underplating of the mush by basalts. This may cause remelting of crystals until the mush may convectively stir and finally erupt as an unzoned, homogenous crystal-rich dacite, known as a monotonous intermediate (Hildreth 1981).

In contrast, others suggested that voluminous intrusive rocks, such as those in large batholiths, do not share the same histories as monotonous intermediates. The plutons may accumulate mostly during low magma flux stages of long-lived volcanic centers. Ignimbrites could occur when power input peaks and allows for the rapid production of voluminous melts, which may preferentially erupt and leave little behind in the plutonic record (Glazner et al. 2004; Tappa et al. 2011; Zimmerer and McIntosh 2012; Mills and Coleman 2013).

The composition, size, shape, and spacing of major intrusive suites has led some workers to suggest a direct connection to large caldera-forming eruptions (Lipman 2007; Bachmann et al. 2007; de Silva and Gosnold 2007). However, it is difficult to reconcile the

genetic link between intrusive rocks and large ignimbrite eruptions because the existing data indicate different magma accumulation rates for the two. Emplacement rates for plutons and intrusive suites are on the order of 0.001-0.0001 km^3/a (Crisp 1984; Matzel et al. 2006; Tappa et al. 2011; Davis et al. 2012; Leuthold et al. 2012). In contrast, magma flux for regions of large ignimbrite activity such as the Altiplano-Puna volcanic complex of the central Andes can episodically be an order of magnitude higher (0.06 km^3/a; de Silva and Gosnold 2007). Numerical modeling of sill intrusion suggests that a magma flux greater than 0.01 km^3/a is required to create enough eruptible magma to feed large (greater than 450 km^3) ignimbrite eruptions (Annen 2009; Schöpa and Annen 2013).

One proposed solution to the silicic magma flux problem is the rejuvenation of magmas that are stored high at crystallinity in the upper crust. The most commonly invoked method of rejuvenation is an event during which mafic magmas underplate a silicic mush, which serves to "defrost" them (Mahood 1990). As the mafic magmas crystallize, heat and volatiles may be released into the overlying mush. Various physical mechanisms that allow for heat transport, and thus rejuvenation, include "convective self-mixing" (Couch et al 2001), "gas sparging" (Bachmann and Bergantz 2003, 2006; Huber et al 2010), and most recently "unzipping" (Burgisser and Bergantz 2011). All of these mechanisms may lead to resorption of crystals until they convect, or "stir" (Huber et al.2012), thus homogenizing the mush and allowing for eruption of a monotonous intermediate.

The Mount Givens Granodiorite of the central Sierra Nevada batholith (Fig. 1) presents an opportunity to resolve some of the relationships between plutonic and volcanic rocks. Its outcrop area is similar in size to the zoned intrusive suites of the batholith (e.g. Tuolumne and Whitney intrusive suites), yet it is more homogenous in both composition and

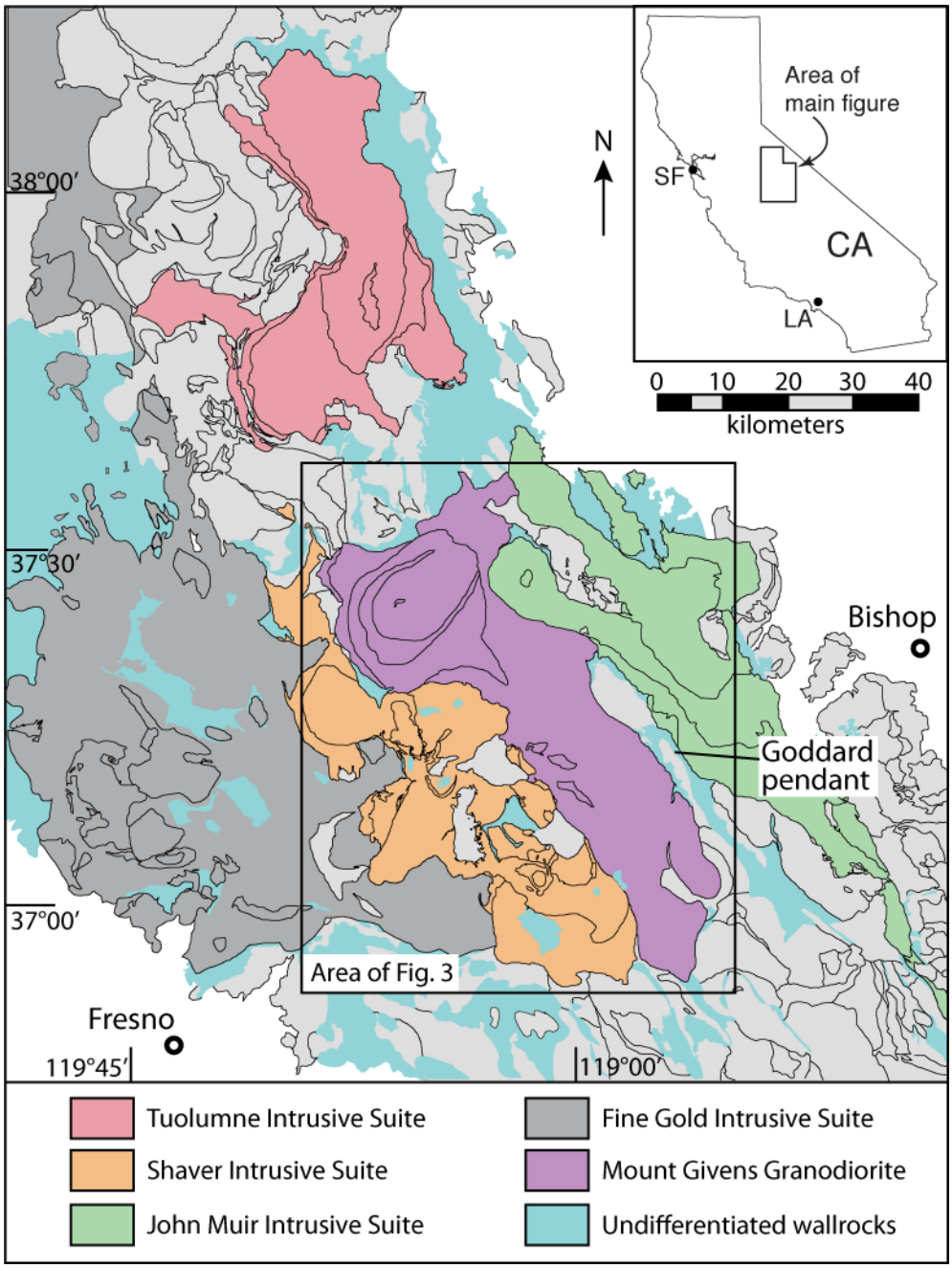

Figure 1. Generalized geologic map of the central Sierra Nevada, CA. Plutons not assigned to major intrusive suites shown in light gray. The John Muir Intrusive Suite of Bateman (1992) has been modified after Davis et al. (2012) to separate the Mount Givens pluton on the basis of the Mount Goddard metamorphic pendant. Map after Bateman (1992), Cruden et al. (1999), Coleman et al. (2004) and Lackey et al. (2008).

texture compared to the zoned suites (Bateman 1992). Previous work on the pluton was undertaken with the notion that the magma was emplaced rapidly (e.g., Bateman and Nokleberg 1978; Tobisch et al. 1993); the longest estimates for its emplacement range from 10^3-10^6 a (McNulty et al. 2000; Petford et al. 2000) suggesting fluxes on the order of 4.5 to 0.0045 km^3/a given the pluton's 4500 km^3 volume. Given its presumed rapid intrusion, large, segmented shape and intermediate composition, the Mount Givens Granodiorite has been postulated to represent an intrusive analog to caldera-forming eruptions that produce monotonous intermediates (Bachmann et al. 2007; de Silva and Gosnold 2007; Lipman 2007; Fig. 2). Specifically, the pluton has been compared to prominent calderas from which large ignimbrites erupted, such as the La Garita (Colorado; Bachmann et al. 2007), La Pacana (Chile; de Silva and Gosnold 2007) and Toba (Indonesia; Lipman 2007) calderas.

I use zircon U-Pb geochronology to evaluate magma emplacement rates in the Mount Givens Granodiorite and its possible link to caldera-forming eruptions. Furthermore, I use knowledge of the pluton's emplacement rate to evaluate models of crystal mush rejuvenation (e.g., Bachmann and Bergantz 2003, 2006; Burgisser and Bergantz 2011) and the effects rejuvenation may have on zircon dissolution. Geochronologic data are also useful in assessing the viability of existing hypotheses for the assembly of the Mount Givens pluton.

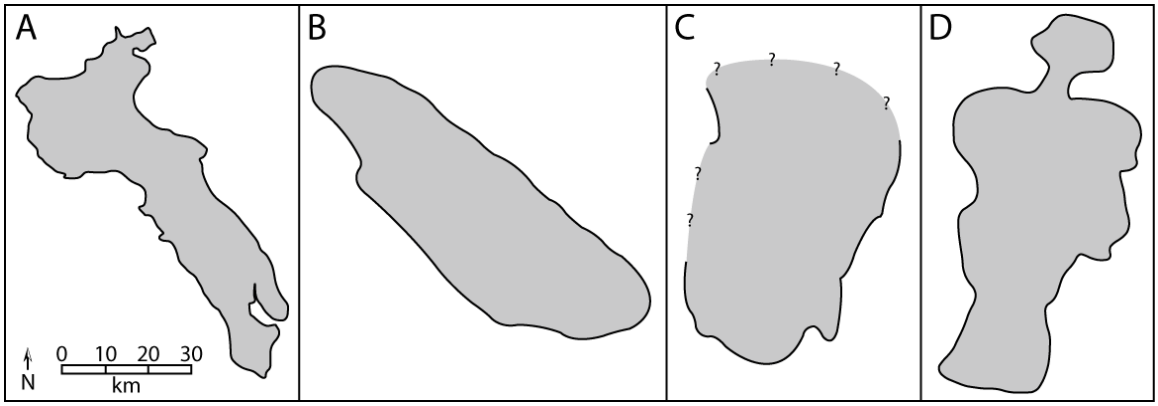

Figure 2. Areal extents of the Mount Givens Granodiorite and three calderas to which it has been compared (Bachmann et al. 2007; de Silva and Gosnold 2007; Lipman 2007). All features at the same scale. **A** Mount Givens Granodiorite (Bateman 1992); **B** caldera of the Youngest Toba Tuff, Indonesia (Chesner 2011); **C** La Pacana caldera, Altiplano-Puna volcanic complex, Chile (queries where caldera margins unknown; Lindsay et al 2001a); **D** La Garita caldera, San Juan volcanic field, Colorado (Bachmann et al. 2002).

II. GEOLOGICAL BACKGROUND

The Sierra Nevada batholith of California is a composite of mostly Cretaceous-age granitoid plutons cropping out over approximately 35,000 km^2 (Fig. 1; Bateman 1992). Many of the plutons in the batholith are grouped into intrusive suites on the basis of their ages, spatial relations, compositions and textures. Suites are characterized by having older, more mafic units at their margins and younger, more felsic units at their cores (Bateman 1992). Zircon U-Pb geochronology demonstrates that these suites were constructed incrementally over 7-16 Ma (Coleman et al. 2004; Frazer et al. 2009; Davis 2010; Memeti et al. 2010; Davis et al. 2012; Lackey et al. 2012). Individual plutons within suites also show evidence for incremental growth over several Ma, including the Half Dome (ca. 4 Ma, Tuolumne Intrusive Suite; Coleman et al. 2004) and Lamarck Granodiorites (ca. 3 Ma, John Muir Intrusive Suite; Davis et al. 2012).

The Mount Givens Granodiorite is located in the central Sierra Nevada batholith (Fig. 3), between the Shaver (106-98 Ma; Frazer et al. 2009) and John Muir (96-84 Ma; Davis et al. 2012) intrusive suites. Although originally included in the John Muir Intrusive Suite (Bateman 1992), Davis et al. (2012) considered the Mount Givens pluton as distinct because it is separated from the rest of the suite by the Mount Goddard metamorphic pendant (Fig. 1).

The Mount Givens Granodiorite is one of the largest single intrusions mapped in the Sierra Nevada batholith (Fig. 1; Bateman 1992), extending approximately 80 km in its longest direction and about 15-30 km across (Fig. 3). Whereas it is similar in area (1500 km^2; Fig. 1) to the zoned Tuolumne and John Muir intrusive suites, published data indicate

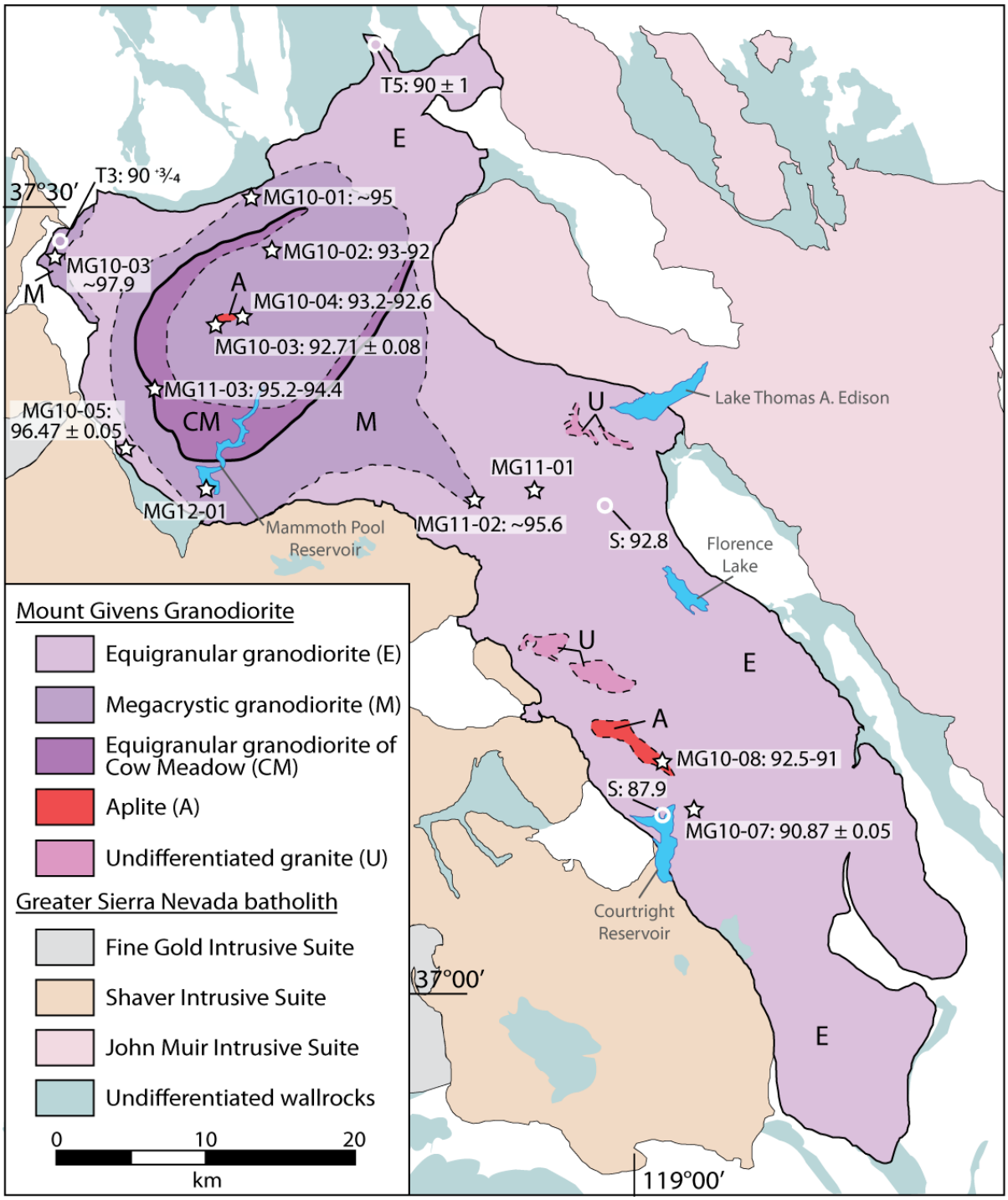

Figure 3. Simplified geologic map of the Mount Givens Granodiorite showing approximate locations and ages (in Ma) of samples dated in this study (stars) and in the literature (circles). Literature age prefixes: S – Stern et al. (1981); T3 – Tobisch et al. (1993); T5 – Tobisch et al. (1995). Thin dashed lines show gradational contacts; heavy black line on outer margin of the granodiorite of Cow Meadow indicates sharp intrusive contact. Individual plutons in the greater Sierra Nevada batholith not shown. Map after Bateman (1992), Cruden et al. (1999) and Lackey et al. (2008).

compositional and textural variations in the pluton are not as significant as those documented in the zoned suites (Bateman and Nokleberg 1978; Bateman and Chappell 1979; Bateman 1992). Bateman and Nokleberg (1978) examined the northern portion of the pluton and determined that most compositional variation occurs within 2 km of the margin. The composition of the pluton ranges from tonalite to granite, but granodiorite and granite dominate (McNulty et al. 2000). Small volumes of aplitic granite are exposed in the center of the exposed northern part of the pluton (granite of Jackass Rock; Bateman and Nokleberg 1978) and in the southern portion near Courtright Reservoir (Fig. 3).

Whereas the southern two-thirds of the pluton are dominated by equigranular granodiorite (Bateman 1992), the bulbous northern end has both equigranular and megacrystic facies (Fig. 3). The largest observed K-feldspar megacrysts are 3 cm long (Bateman and Nokleberg 1978; McNulty et al. 2000). A horseshoe-shaped body of equigranular granodiorite (referred to herein as the granodiorite of Cow Meadow; Bateman et al. 1971) is found within the megacrystic facies and has been mapped with a sharp outer contact and a gradational inner contact (Fig. 3; Bateman et al. 1971; Bateman and Nokleberg 1978; Bateman 1992; McNulty et al. 2000). All other contacts between textural and compositional phases are gradational (Bateman and Nokleberg 1978).

Published zircon U-Pb ages for the Mount Givens Granodiorite range from 92.8 to 87.9 Ma (Stern et al. 1981; Tobisch et al. 1993; 1995). However, these bulk zircon analyses are generally discordant and were not determined using modern thermal annealing and chemical abrasion techniques (Mattinson 2005). Many workers consider the pluton to have intruded around 90 Ma (e.g., Tobisch et al. 1993; 1995; Renne et al. 1993; Gilder and McNulty 1999; McNulty et al. 2000).

Most existing work on the pluton suggests it was assembled rapidly. Bateman and Nokleberg (1978) proposed the pluton was emplaced as a large, fractionally crystallizing magma body similar to the Tuolumne Intrusive Suite (Bateman and Chappell 1979), with aplite bodies in the northern and southern parts of the pluton crystallizing last. Bateman (1992) argued that the concentric structure of the northern portion might be the result of magma resurgence and folding.

McNulty et al. (2000) suggested a rapid (10^3-10^6 a), multi-stage assembly of the Mount Givens Granodiorite via diking and sill formation (e.g., Cruden 1998; Petford et al. 2000). Using anisotropy of magnetic susceptibility (AMS) methods, they proposed the construction of the Mount Givens pluton occurred as follows: (1) equigranular granodiorite magma ascended in N-S oriented dikes to the upper crust from a middle- to lower-crustal magma chamber. Ascent occurred in the southern part of the pluton, followed by lateral flow toward the northern portion. Space was created via floor downdrop into the emptying chamber below; (2) megacrystic granodiorite magma ascended via dikes in the northern part of the pluton and underplated the equigranular magma. Lateral flow is indicated by the "tongue" of megacrystic granodiorite that extends toward the central part of the pluton (Fig. 3); (3) another pulse of equigranular magma (granodiorite of Cow Meadow) underplated the megacrystic magma. Floor downdrop ceased and the northern part of the pluton bulged up and outward, flexing the three sills; (4) ring diking allowed the Cow Meadow magma to ascend further, resulting in a sharp, arcuate contact and subvertical magnetic lineations. This action could have resulted in a trap-door style caldera at the paleosurface.

III. METHODS

Twelve 5-kg samples were collected from parts of the Mount Givens Granodiorite (Fig. 3) mapped as equigranular or porphyritic granodiorite or aplitic granite. Sample MG10-01 was collected in an area mapped as megacrystic granodiorite, but it is equigranular. Conversely, sample MG10-07 was collected in an area mapped as equigranular granodiorite, but it is megacrystic. Six samples were collected along a transect across the northern portion of the pluton including the central aplitic granite of Jackass Rock (Bateman and Nokleberg 1978). Four samples were collected from different textural and compositional phases in the middle and southern portions of the pluton. Sample MG11-04 was collected from the same general locality as a sample dated by thermal ionization mass spectrometry using mg-sized fractions, which yielded an age of 90 +3/-4 Ma (Tobisch et al. 1993).

Zircon was extracted from the samples by standard crushing (jaw crusher and disc mill) and gravimetric (water table and heavy liquids) techniques. Grains representative of the populations' sizes and morphologies were selected by hand under a binocular microscope from the non-magnetic split on a Frantz magnetic separator operated at 1.5 A and 10° side tilt. Zircon grains from all samples were thermally annealed at 900°C for 48 hours and all but one sample were chemically abraded in 29M HF acid for 16 hours at 220°C to remove mineral inclusions and zones affected by radiation damage that are subject to Pb-loss (Mattinson 2005). Zircons from sample MG10-03 (granite of Jackass Rock) were abraded for 16 hours at only 180°C to preserve more of the sparse, typically small grains. Fractions consisting of either a single zircon or an isolated zircon tip were spiked with a ^{205}Pb-^{233}U-^{236}U tracer

(Parrish and Krogh 1987) and dissolved in 29M HF acid following a procedure modified after Krogh (1973) and Parrish (1987). Anion exchange (HCl) column chromatography was used to isolate U and Pb from the dissolved solution.

Analyses of U and Pb were completed using a VG Sector 54 thermal ionization mass spectrometer at the University of North Carolina at Chapel Hill. Uranium was run on single Re filaments either as a metal, after loading in graphite and H_3PO_4, or as an oxide, after loading in silica gel. Lead was loaded in silica gel on single Re filaments. Both U and Pb were analyzed in single-collector peak-switching mode using a Daly ion-counting system. Data processing and age calculations were completed using the applications Tripoli and U-Pb_Redux developed as part of the EARTHTIME initiative (Bowring et al. 2011; McLean et al. 2011). Decay constants used were $^{238}U = 1.55125 \times 10^{-10}$ a^{-1} and $^{235}U = 9.8485 \times 10^{-10}$ a^{-1} (Steiger and Jäger 1977).

Corrections for initial Th/U disequilibrium (Schmitz and Bowring 2001) were made using U-Pb_Redux. An assumed magmatic Th/U ratio of 3.7 was used based on an average of six whole rock analyses of Th and U for the Mount Givens Granodiorite (Th/U range: 1.6-5.7; Dodge et al. 1982; Noyes et al. 1983). Sample KMG-20 of Noyes et al. (1983) is excluded from the average Th/U calculation because its location is undetermined. A Th/U ratio of 3.7 is also reasonable because it is the average Th/U ratio of all granodiorites in the Sierra Nevada batholith according to data in the NAVDAT database (www.navdat.org). The difference between an uncorrected $^{206}Pb/^{238}U$ weighted mean age and an age that has been corrected for a magmatic Th/U ratio of 3.7 is approximately 95 ka in these samples. Variation in calculated ages due to different Th/U ratios found in the pluton is minor; the

disparity in weighted mean ages corrected for Th/U ratios from 1.6 to 5.7 is approximately 20 ka.

IV. RESULTS

Zircon fractions from all samples contain few inclusions. Cathodoluminescence (CL) images of representative grains from each sample (except for MG10-03, which was not imaged) indicate typical magmatic oscillatory zonation (Appendix 1; Corfu 2003). CL imaging also revealed the presence of possible inherited cores in some zircons; visual inspection suggests that MG10-01, MG10-02, MG10-04, MG11-01 and MG11-03 may have more inherited cores than other samples.

All fractions are concordant after correcting for initial Th/U disequilibrium (accounting for analytical and decay constant uncertainties; Appendix 2; Fig. 4). Thus, I use the weighted mean $^{206}Pb/^{238}U$ age as the best estimate for crystallization ages of the samples in which there is a tight distribution of fraction ages. Several samples show significant scatter in individual fraction ages beyond analytical uncertainty; these samples are only given an approximate crystallization age. However, when a subset of three or more overlapping fractions is present at the lower age limit for the sample, a weighted mean age is reported.

Northern part of the Mount Givens Granodiorite

Three of the four oldest crystallization ages come from samples collected near the outer margins of the Mount Givens Granodiorite. The oldest sample, MG11-04, was collected near the northwest margin of the pluton in a small area mapped as megacrystic granodiorite. It has 2 cm K-feldspar megacrysts, which were the largest observed for any sample in this study. It yielded an age of ca. 97.9 Ma with one fraction that is ca. 500 ka

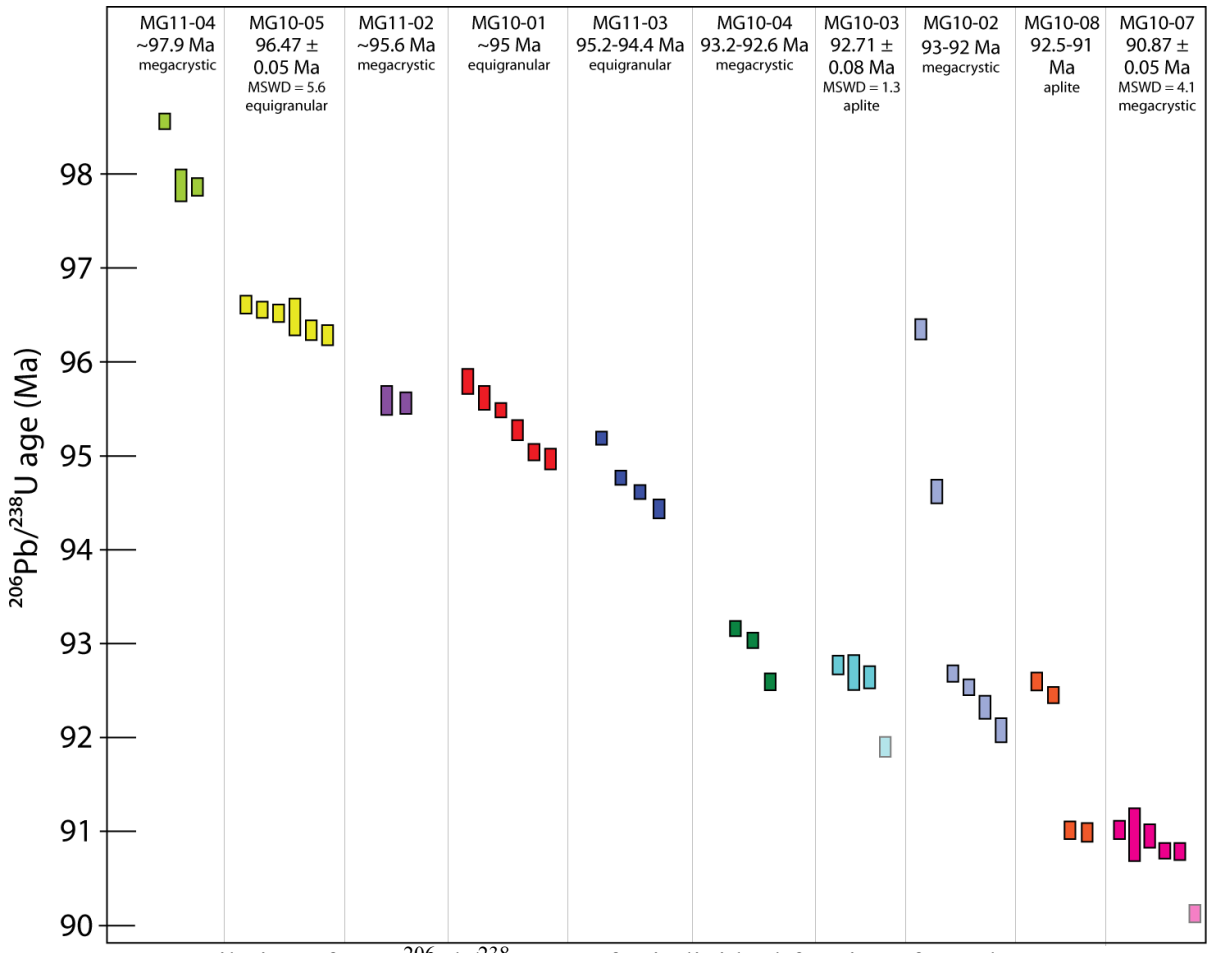

Figure 4. Compilation of new $^{206}Pb/^{238}U$ ages for individual fractions from the Mount Givens Granodiorite. Only fractions that are concordant within analytical uncertainty are included. For clarity, fraction F-5 (~102.6 Ma) from sample MG10-02 is not shown. Weighted mean ages are calculated only for samples with three or more overlapping fractions that are interpreted to represent crystallization age; fractions not included in weighted mean calculations are faded out. All other sample ages are estimates. Weighted mean ages and 2σ analytical error calculated using the application U-Pb_Redux (Bowring et al. 2011; McLean et al. 2011). All fraction ages are corrected for initial Th-disequilibrium assuming a magmatic Th/U ratio of 3.7.

older than the others. This sample was collected near the location of the 90 +3/-4 Ma sample of Tobisch et al. (1993).

Sample MG10-01 was collected from outcrop mapped as megacrystic facies at the northern margin but the sample is equigranular in texture. Individual fraction ages spread over ca. 1 Ma of concordia, from 96-95 Ma. On the basis of three overlapping fractions at the lower end of the age spectrum, I interpret its crystallization age to be ca. 95 Ma. Sample MG10-05 was collected at the southeastern margin of the pluton. It is equigranular in texture and six zircon fractions yielded a weighted mean age of 96.47 ± 0.05 Ma with an mean square of weighted deviates (MSWD) of 5.6.

Samples MG10-02, MG10-03, MG10-04 and MG11-03 were collected inboard of the margins of the bulbous northern part of the pluton. The observed textures of all these samples matched the textures mapped for the sample locations by Bateman (1992; Fig. 3). All of the samples are younger than those collected at the margins.

Sample MG11-03 was collected in the equigranular granodiorite of Cow Meadow near the mapped location of its intrusive contact with the megacrystic facies. However, I did not observe the contact at that locality. Four fractions range from 95.2-94.4 Ma.

Samples MG10-03 and MG10-04 were collected approximately 1 km apart from each other in the core of the northern part of the pluton. Sample MG10-03 was collected from the granite of Jackass Rock, a body of fine-grained aplitic granite with a color index near zero. Three overlapping fractions give a weighted mean age of 92.71 ± 0.08 Ma with an MSWD of 1.3. A fourth fraction yields an age of ca. 91.9 Ma. Sample MG10-04, collected in the nearby megacrystic facies, has three fractions ranging from 93.2-92.6 Ma.

The final rock dated from the northern portion of the pluton is sample MG10-02, a megacrystic granodiorite. It yields a complicated age spectra, with seven concordant fractions ranging from 102.6-92 Ma. The four youngest fractions cluster from 93-92 Ma.

Central part of the Mount Givens Granodiorite

One sample (MG11-02) was collected in the southern part of the megacrystic granodiorite. Uranium-lead data from two fractions indicate a crystallization age of ca. 95.6 Ma, similar to ages from marginal samples in the northern part of the pluton.

Southern part of the Mount Givens Granodiorite

Whereas the entire southern portion of the pluton was previously mapped as equigranular (Bateman 1965; Bateman 1992), sample MG10-07 is megacrystic. Five fractions overlap for a weighted mean age of 90.87 ± 0.05 Ma and an MSWD of 4.1. One fraction falls below the main grouping with an age of ca. 90.15 Ma.

Sample MG10-08 was collected from an area mapped as aplitic granite and was generally finer-grained and more felsic (CI = ~2) than nearby granodiorites. It also contains 1-cm K-feldspar phenocrysts. Fraction ages occurred in two groupings: one group near 92.5 Ma, and a second group near 91.0 Ma.

V. DISSCUSSION

Zircon recycling in the Mount Givens Granodiorite

Improvements in analytical methods for TIMS U-Pb zircon dating, including thermal annealing, chemical abrasion (Mattinson 2005) and error treatment (Schmitz and Schoene 2007; McLean et al. 2011) revealed that spread along concordia is a common occurrence in plutonic rocks (e.g., Coleman et al. 2004; Matzel et al. 2006; Tappa et al. 2011; Davis et al. 2012; Rioux et al. 2012). This led workers to question what causes age dispersion and what a set of zircon ages means (Miller et al. 2007; Schaltegger et al. 2009).

The significance of analyses that are hundreds to thousands of years older (or younger) than the main age group is unclear. Older ages could be the result of prolonged (antecrystic) zircon growth in a crystal mush that was periodically rejuvenated by fresh magmas (Miller et al. 2007). This scenario suggests a direct genetic link between older and younger zircons. Conversely, the ages could represent variable incorporation of minor amounts of inherited (xenocrystic) zircon that was introduced into magma batches as they ascended through different levels of the crust (Schaltegger et al. 2009). This could result in a similar spread along concordia but does not necessitate a long-lived magma mush system at the level of emplacement.

Despite the development of the thermal annealing-chemical abrasion technique (Mattinson 2005), zircons may still be affected by Pb-loss, causing spread along concordia. Age dispersion could be minimized (in the case of Pb-loss in an antecrystic zircon) or enhanced (in the case of Pb-loss in an autocrystic zircon), making zircon age spectra more

difficult to interpret. Though U-Pb dating of titanite from the same samples may shed light on when final zircon crystallization occurred (Schaltegger et al. 2009; Davis et al. 2012), I did not undertake those analyses in this study. As such, in samples with significant spread along concordia I choose to assign only approximate crystallization ages, favoring the younger end of the age spectrum (e.g., MG10-01). Though I aggressively chemically abraded zircons in this study, there were infrequent fractions far below the dominant age groupings or spreads in some samples (e.g., MG10-07). I interpret these to be the results of Pb-loss – perhaps even Pb-loss that occurred during chemical abrasion. In samples with consistent overlapping ages I assign a weighted mean age (e.g., MG10-05).

The source(s) of the remaining spread in some of the samples is unclear, but I may make some inferences based on their age spectra. Miller et al. (2007) posited that zircons might be recycled (and thus result in age spread in single samples) as high-crystallinity magmas mix with new inputs and zircons are redistributed in the crystal mush. However, the results suggest that this redistribution did not occur on the pluton-scale, and if it did occur it was likely limited to local mixing. Age spectra for the youngest (MG10-07) and oldest (MG11-04) samples in the pluton, 60 km apart, do not show overlap. Sample MG10-02 has one fraction with an age of 96.3 ± 0.1 Ma and another at 94.5 ± 0.1 Ma, which bracket all the fraction ages from sample MG10-01, ~3 km away, but do not overlap (Fig. 4). However, overlap does occur between samples 1 km apart: MG10-03, an aplitic granite, is similar in age to sample MG10-04, a megacrystic granodiorite from which the aplite could have been derived.

I suggest that incorporation of zircons in ascending magmas, prior to reaching emplacement level, could have contributed to the spread in zircon ages observed here

(Schaltegger et al. 2009). If ascent was rapid (e.g., Petford et al. 2000) and magmas cooled rapidly (Davis et al. 2012), they may preserve inherited zircons incorporated during the ascent. Trace element analyses of zircons using the ID-TIMS-TEA method (Schoene et al. 2010) may be useful in helping determine the provenance of the zircons in future work.

Emplacement models for the Mount Givens Granodiorite

Many of the existing models for the formation of the Mount Givens Granodiorite call for rapid emplacement of the pluton. For example, Bateman and Nokleberg (1978) concluded that compositional patterns preserved in the Mount Givens pluton were the result of fractional crystallization of a large magma body (similar to interpretations of the Tuolumne Intrusive Suite [Bateman and Chappell 1979]). Modeling simple conductive cooling of large magma intrusions predicts a range of U-Pb zircon ages amongst samples of less than 1 Ma (Glazner et al. 2004). The age data presented here show a range of 6 Ma amongst samples in the northern portion of the pluton alone, making single-batch intrusion unlikely.

Tobisch et al. (1993) followed the rapid emplacement model, using the 90 +3/-4 Ma age for a sample in the northwestern part of the pluton to also represent its age 60 km south near Courtright Reservoir. However, sample MG11-04, collected near Tobisch et al.'s (1993) sample, yielded an age of 97.9 Ma. The large age discrepancy between these two samples may be real, or may be the result of unresolved Pb-loss in the bulk zircon fractions by Tobisch et al. (1993), which were analyzed before development of techniques to minimize this problem.

McNulty et al. (2000) also called for rapid assembly of the Mount Givens Granodiorite (10^3-10^6 a) based on modeling of piston sinking mechanisms by Cruden (1998). This range includes the preferred filling time for the Mount Givens pluton of 10^5 a by Petford

et al. (2000). Using AMS data, McNulty et al. (2000) suggested magma ascended rapidly in dikes and spread laterally, resulting in large sills of alternating texture. Further ring diking in the north would have allowed the structurally lowest equigranular magma to ascend, resulting in the sharp outer contact of the granodiorite of Cow Meadow. This hypothesis predicts that each textural facies would have internally similar ages throughout the pluton.

However, the geochronologic data suggest that it is unlikely that the different textural facies were intruded in discrete events. Instead, equigranular samples dated here span at least 2 Ma. The age span for the megacrystic facies includes the 7 Ma range for the entire pluton and thus overlaps with the equigranular facies. Finally, the granodiorite of Cow Meadow does not appear to be the youngest part of the Mount Givens pluton. Instead, its 94.7 Ma age is between the ages of the margin and core of the pluton (Fig. 3).

Interpretations of magmatic and magnetic structures in plutons

McNulty et al. (2000) found that magnetic foliations are subparallel to magmatic foliations observed in the field, which is a common observation (King 1966; Gulliet et al. 1983; Cruden and Launeau 1994; de Saint Blanquat and Tikoff 1997; Cruden et al. 1999; Tikoff et al. 2005). They inferred that magnetic foliations and lineations are a result of magmatic processes due to the presence of a strongly concentric pattern of foliations in the northern portion of the pluton, and separate zones of subvertical and subhorizontal magnetic lineations in the southern portion. Neither of these observations is compatible with regional deformation patterns, which were oriented NW-SE (Bateman 1992; Tikoff and de Saint Blanquat 1997; de Saint Blanquat et al. 2011). Thus, they attributed magmatic and magnetic structures in the pluton to magma flow processes. However, there are at least two alternative mechanisms for the generation of aligned mineral grains, including crystallization in a

thermal gradient (Huang et al. 2009; Lundstrom 2009; Lundstrom et al. 2011) and realignment and recrystallization during thermal cycling (Mills et al. 2011).

Thermal cycling is a process that is likely important during pluton construction because incremental emplacement should cause an oscillating temperature pattern through time (Annen et al. 2006; Davis and Coleman 2008; Annen 2009). Davis et al. (2012) used U-Pb (zircon and titanite) and $^{40}Ar/^{39}Ar$ (hornblende and biotite) thermochronology to demonstrate that magmas in the John Muir Intrusive Suite (Fig. 1) cooled rapidly from zircon saturation through Ar closure in hornblende, then remained elevated above biotite closure for 2-11 Ma. They suggested that the prolonged period between hornblende and biotite dates could have been the result of thermal cycling due to younger pluses of magma reheating older pulses above biotite Ar closure temperatures.

It seems likely that thermal cycling (and by extension, migrating thermal gradients) would have occurred in the Mount Givens Granodiorite. The pluton shows a large spread in U-Pb zircon ages, including a general decrease in age from margin to core in the northern portion (Fig. 3). This suggests incremental emplacement of small batches of magma, which could cause oscillating temperatures in older magma batches and thus realignment of minerals important to AMS such as magnetite and (to a lesser extent) hornblende.

Origin of the sharp intrusive internal contact

The presence of an obvious internal contact on the outer margin of the equigranular granodiorite of Cow Meadow (Fig. 3) was interpreted as a late intrusion of magma into the Mount Givens system, perhaps due to resurgence or late stage ring-diking (Bateman et al. 1971; Bateman 1992; McNulty et al. 2000). However, the geochronologic data presented here indicate that the age of the granodiorite of Cow Meadow is intermediate between the

pluton's western margin and its core. I hypothesize that the origin of the sharp contact and the pluton's alternating textural facies may be due to repetition of magma emplacement cycles (Fig. 5).

The cycles begin with the oldest magmas intruding cooler wallrocks, leading to rapid cooling and preservation of equigranular texture. As magmatism continues, the thermal gradient may increase; furthermore, successive inputs of magma will lead to thermal oscillations. The steady transition to higher, cycling temperatures may result in both the slightly younger megacrystic facies inboard of the equigranular facies, as well as the gradational contact between them (Johnson and Glazner 2010).

The sharp contact between the megacrystic facies and the outer granodiorite of Cow Meadow may be a result of the magmatic cycle ending, allowing the system to cool. When a new cycle began, Cow Meadow magma batches were emplaced against cooler wallrock, which in this case was megacrystic granodiorite. This thermal juxtaposition could result in rapid cooling, preserving the sharp intrusive contact and the equigranular texture observed in the granodiorite of Cow Meadow. The magmatic cycle continued, repeating the process of a gradual thermal gradient increase along with thermal cycling, producing another gradational contact into the innermost megacrystic granodiorite. The concentric structure of the contacts may be due to doming and flexing in the northern portion of the pluton as it grew, resulting in a laccolith-type geometry.

Magma fluxes in plutons and large ignimbrites

The Mount Givens Granodiorite has been cited as a possible intrusive analog to ignimbrites because of its composition, structure, and volume (Fig. 2; Bachmann et al. 2007; de Silva and Gosnold 2007; Lipman 2007; Bachmann and Bergantz 2008). Specifically, the

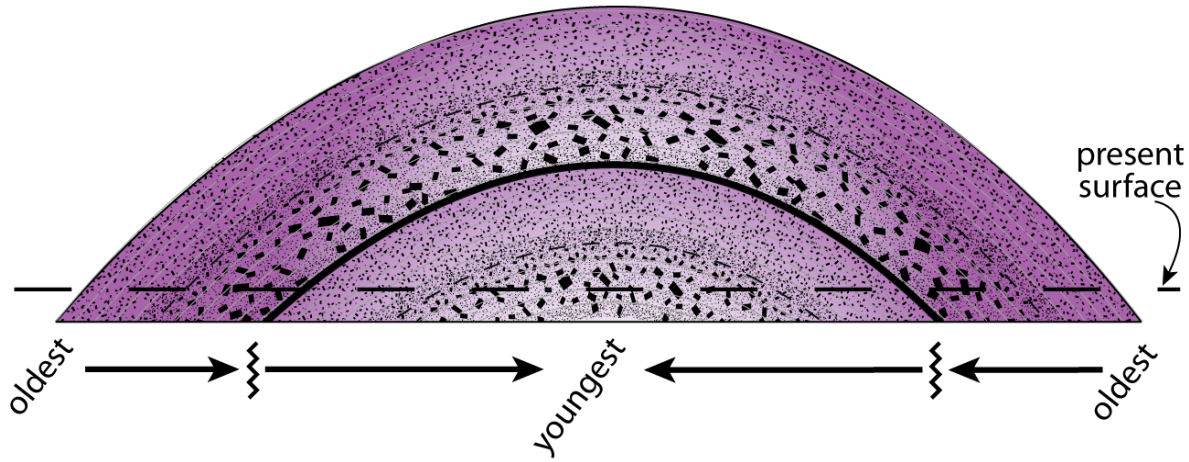

Figure 5. Schematic representation of emplacement and textural facies development in the northern part of the Mount Givens Granodiorite. Potassium feldspars are represented by black boxes (not to scale). Individual magmatic inputs are bordered by light gray lines (not to scale). No vertical scale is implied. Gradational contacts between textural facies are indicated short black dashed lines; sharp intrusive contact is shown with a heavy black solid line. Present day erosional surface shown by long black dashed line. In this model, the magmatic cycle begins with the oldest magmas rapidly crystallizing into an equigranular texture. As magma inputs buffer the system, they may stay above the minimum temperature required for coarsening, allowing development of megacrystic texture and gradational contacts between textural facies (Johnson and Glazner 2010). A temporal break in magma emplacement is indicated by the jagged black lines. This break allows T to decrease such that when the magma input cycle begins again, the older megacrystic granodiorite is cool "wallrock". The new magmas crystallize rapidly with equigranular texture, followed by the gradational development of megacrystic texture. The concentric pattern exposed today is the result of a doming of the sills as the northern portion grew into a laccolith-type structure.

pluton has been likened to large (>2000 km^3) homogenous crystal-rich dacites known as monotonous intermediates (Hildreth 1981). Bachmann et al. (2007) speculated that eruptions from the growing Mount Givens pluton were likely and thus the original vertical extent of the magma was greater than 5 km (McNulty et al. 2000), implying that even the source of the 5000 km^3 Fish Canyon Tuff may have left behind a large pluton. De Silva and Gosnold (2007) suggested that pluton growth and large ignimbrite generation occur at the same rates and are thus directly linked, based on the similarity of their calculated intrusion rates for the Altiplano-Puna volcanic complex (0.012-0.06 km^3/a) to Petford et al.'s (2000) filling rate model for the Mount Givens pluton (0.032 km^3/a).

To evaluate these hypotheses, I calculate an average magma flux for the Mount Givens Granodiorite of 0.0006 km^3/a by using the age range of the Mount Givens pluton established here (7 Ma), the area of the pluton (1500 km^2) and the exposed vertical relief as a proxy for thickness (3 km). Using McNulty et al.'s (2000) thickness estimate of 5 km (based on AMS data) yields a flux of 0.0007 km^3/a. These rates are similar to magma fluxes calculated for other plutons in the Sierra Nevada (Coleman et al. 2004; Davis et al. 2012; Lackey et al. 2012) and elsewhere (Matzel et al. 2006; Tappa et al. 2011; Leuthold et al. 2012; Mills and Coleman 2013). However, this is 1-2 orders of magnitude lower than fluxes observed for large-volume ignimbrites (Schmitz and Bowring 2001; Schmitt et al. 2002; Vazquez and Reid 2004; Bachmann et al. 2007; Crowley et al. 2007), which record zircon growth on the order of 10^5 a rather than 10^6-10^7 a.

Numerical modeling by Annen (2009) indicates that constant magma fluxes greater than 0.01 km^3/a are necessary to develop magma chambers capable of supporting large (>450 km^3) eruptions. Schöpa and Annen (2013) considered the effects of variable magmatic fluxes

through time, yielding similar results. Keeping the average magmatic flux of the Tuolumne Intrusive Suite constant at 0.0014 km^3/a over 7 Ma, a mobile magma chamber greater than 450 km^3 can only be generated when there is a transient pulse of at least 0.05 km^3/a, delivering more than 1000 km^3 of magma to emplacement level over 40 ka. These modeled fluxes are in agreement with the fluxes calculated by de Silva and Gosnold (2007) for flare-ups defined by large ignimbrite eruptions in the Altiplano-Puna volcanic complex. Thus, the difference in fluxes between large plutons and similarly-sized ignimbrites might: 1) indicate the hypothesized link between the two rock types—that plutons are either unerupted equivalents or complementary residua of large ignimbrites—is incorrect, or 2) be a reflection of the proposed differences in their T-t histories.

Zircon dissolution during mush rejuvenation

The observation that phenocrysts in ignimbrites often record heating events prior to eruption (e.g., Bachmann and Dungan 2002; Bachmann et al. 2002; Wark et al. 2007; Molloy et al. 2008; Shane et al. 2008; Bachmann 2010) led to the hypothesis that monotonous intermediates and other large ignimbrite eruptions occur when long-lived, crystal-rich silicic mushes (50+% crystals) are underplated by mafic magmas and rejuvenated (e.g., Mahood 1990; Bachmann et al. 2002). Though the proposed mechanisms by which the mushes may be revived differ (Bachmann and Bergantz 2003, 2006; Huber et al. 2009, 2010, 2012; Burgisser and Bergantz 2011), the final outcome—eruption—is the same. If heating events do not successfully rejuvenate a magma mush, then it may cool completely to form a granodiorite pluton (Bachmann et al. 2007).

If monotonous intermediates and plutons were both once large crystal mushes, and plutons are simply crystallized mushes with multi-Ma zircon age spans, then the zircons that

would have recorded the same multi-Ma growth of the mush must be dissolved prior to eruption. The difference in apparent magmatic fluxes calculated using zircon geochronology for large plutons and monotonous intermediates would thus be a result of their different T-t histories.

Using Watson's (1996) equation for the instantaneous dissolution of a spherical zircon, I modeled the effects of hypothetical heating events on zircons with initial radii from 30-120 μm, which are reasonable sizes for zircons in large ignimbrites (Bindeman 2003). The parameters used were similar to those suggested for the Fish Canyon magma. Temperatures were increased from 715-760°C (Bachmann and Dungan 2002) monotonically. Since proposed rejuvenation times range from less than a few centuries (Burgisser and Bergantz 2011) to 200 ka (Bachmann and Bergantz 2003), I used the equation iteratively over timespans ranging from 1 ka to 200 ka.

In order to maximize dissolution I began with the assumption of no (zero) dissolved Zr in the melt initially, and any Zr derived from the dissolving zircons was immediately removed from the system. Adding initial Zr to the magma and increasing the Zr content of the magma in response to zircon dissolution would slow zircon dissolution and may even yield zircon precipitation. The lack of dissolved Zr in the model also accounts for the compositional differences between granodiorite magmas ($M \approx 1.7$; where $M \equiv (2Ca + Na + K)/(Si \cdot Al)$) and the peraluminous experiments upon which the dissolution equation is based ($M \approx 1.3$; Watson 1996), which do not dissolve zircon as readily as metaluminous magmas. For example, at 715°C the Zr saturation concentration is 86 ppm when $M = 1.7$, but it is 60 ppm when $M = 1.3$.

Results suggest that it is possible to fully dissolve zircons with radii up to nearly 100 μm under the favorable conditions of this model (Fig. 6A). A hypothetical heating event over the maximum 200 ka with no dissolved Zr present in the melt results in complete dissolution of the 10, 25, 50 and 75 μm-radius model zircons. However, a zircon with an initial radius of 100 μm would survive the event with a final radius of 28 μm. Exposing zircons to the same temperature range using the shorter rejuvenation timespans (<1 ka) that have been recently proposed (Burgisser and Bergantz 2011) results in negligible dissolution (Table 1).

The addition of Zr to the melt in this model results in less dissolution (Fig. 6A). With 60 ppm Zr held constant throughout the model (i.e., as the temperature increases, [Zr] is constant and the system becomes Zr-undersaturated), the 75 μm zircon survives over 200 ka, as compared to the Zr-free case. The addition of Zr also limits dissolution over shorter timescales, as the 10 μm zircon requires nearly twice as much time to fully dissolve.

If the rejuvenation event brings the temperature of the melt up to higher temperatures, more dissolution is possible. For example, if the temperature rises to 800°C (Lund Tuff; Maughan et al. 2002), larger model zircons will dissolve over the longer time paths (Fig. 6B). However, the increased temperature has little effect on zircons during the shorter rejuvenation events and dissolution is further inhibited with the addition of Zr to the melt (Table 1).

These results suggest that the effects rejuvenation events have on zircons present in their systems may be limited, particularly because the parameters used in these models were chosen to maximize dissolution. Real systems would likely dissolve even less zircon than indicated here. For example, these models assume the zircon is interacting with an infinite reservoir into which Zr may diffuse. However, in real systems the zircons likely interact with

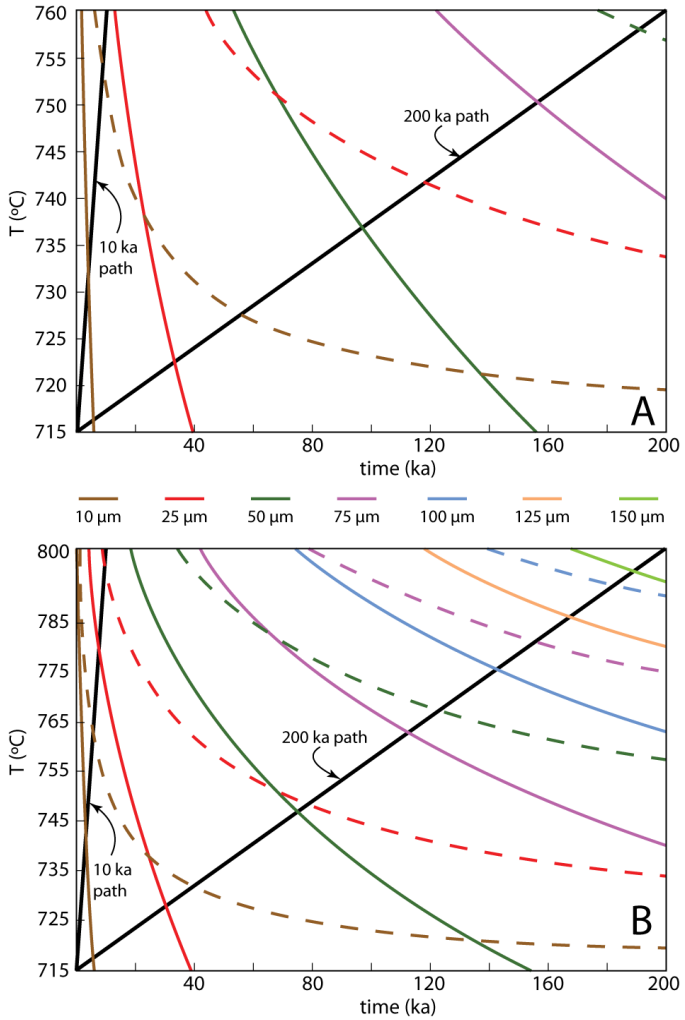

Figure 6. Temperature-time plots contoured for timing of dissolution of spherical model zircons based on the parameterization of Watson (1996). Contours indicate the T and t at which a zircon of a given radius will fully dissolve assuming a linear T-t path beginning at the origin (T = 715ºC; t = 0 ka). Solid colored lines show results determined with zero dissolved Zr in the model; dashed colored lines are for 60 ppm dissolved Zr held constant in the melt. At any point below a given curve, that zircon will survive without complete dissolution. Heavy black lines indicate the maximum proposed heating path (200 ka; Bachmann and Bergantz 2003), and a short heating path (10 ka). Note that Burgisser and Bergantz suggest rejuvenation times <1 ka. Any colored lines that intersect these paths indicate complete dissolution of model zircon. **A** Modeling based on the temperature range proposed for the Fish Canyon Tuff (Bachmann and Dungan 2002). Over the long heating path, zircons with radii <100 µm will not survive when no dissolved Zr is present, whereas 60 ppm Zr limits complete dissolution to zircons ≤50 µm. The 10 ka heating path only permits very small (<10 µm) zircons to fully dissolve. This short path is longer than the rejuvenation timescales proposed by Burgisser and Bergantz (2011) **B** Modeling with the upper temperature (800°C) based on maximum temperature estimates for other monotonous intermediates (Chesner 1998; Lindsay et al. 2001b; Maughan et al. 2002). Larger zircons dissolve than for the Fish Canyon Tuff, but short rejuvenation timescales will fully dissolve only the smallest (10-25 µm) zircons.

limited melt reservoirs (~1.5 mm), which would discourage dissolution (Watson 1996). Furthermore, the recent preferred timescales for the rejuvenation of even the largest crystal-rich mushes such as the Fish Canyon Tuff are on the order of centuries to 10 ka (Burgisser and Bergantz 2011; Huber et al. 2012), which should preserve many of the initial zircons that would record mush growth (Fig. 6; Table 1).

These results are supported by the presence of ancient xenocrystic zircon cores in monotonous intermediates (Lanphere and Baadsgaard 2001; Schmitt et al. 2002) and other large ignimbrites (Zimmerer and McIntosh 2012). It is improbable that heating events preceding ignimbrite eruption would selectively dissolve zircons recording long-term (up to 10 Ma) growth of a "proto-ignimbrite" but would preserve much older zircons that were not derived from the active magmatic system. In order for such rejuvenation events to successfully dissolve zircon, the events must be hot, long-lived, and very Zr-poor.

Large mafic sills in silicic batholiths

A fundamental requirement of the hypotheses for erupting a crystal mush is the presence of hot basalt to underplate and rejuvenate the mush. Estimates for the volumes of basalt necessary vary widely depending on the mechanism by which the rejuvenation occurs. For example, much more mafic magma is required for "gas sparging" (Bachmann and Bergantz 2003) than for "unzipping" (Burgisser and Bergantz 2011).

Using similar input parameters to Bachmann and Bergantz (2003) for gas sparging (Appendix 3), I find that 1550 km^3 of mafic magma would be necessary to remobilize a hypothetical Mount Givens magma. The amount of mafic magma necessary for unzipping is much less, with a maximum sill thickness for the most viscous silicic magmas calculated to be 83 m, resulting in ~125 km^3 of mafic magma if the entire 1500 km^2 Mount Givens pluton

Table 1 Results of spherical zircon dissolution modeling

r_o (μm)	1 ka	50 ka	100 ka	150 ka	200 ka
		715-760°C, 0 ppm Zr in melt			
10	7.3	-	-	-	-
25	24.1	-	-	-	-
50	49.5	14	-	-	-
75	74.7	58	32	-	-
100	99.8	88	73	55	28
125	124.8	115	105	93	78
150	149.8	142	133	125	115
max[a]	6.8	48	68	83	96
		715-760°C, 60 ppm Zr in melt			
10	9.2	-	-	-	-
25	24.7	-	-	-	-
50	49.9	42	33	19	-
75	74.9	70	65	59	53
100	99.9	96	93	89	85
125	124.9	122	119	116	113
150	150.0	148	145	143	140
max[a]	3.8	27	38	46	54
		715-800°C, 0 ppm Zr in melt			
10	-	-	-	-	-
25	22.1	-	-	-	-
50	48.6	-	-	-	-
75	74.1	-	-	-	-
100	99.3	57	-	-	-
125	124.5	94	46	-	-
150	149.5	126	95	48	-
max[a]	11.6	82	116	142	164
		715-800°C, 60 ppm Zr in melt			
10	5.3	-	-	-	-
25	23.5	-	-	-	-
50	49.3	-	-	-	-
75	74.5	45	-	-	-
100	99.6	80	53	-	-
125	124.7	110	92	70	35
150	149.8	137	124	108	90
max[a]	8.5	59.9	85	104	119.7

[a] radius (μm) of the largest zircon that will completely dissolve using given parameters

were underplated. Under Burgisser and Bergantz's (2011) "standard conditions", a sill just 5.3-m thick would unzip a 2-km thick mush. If the 4500 km^3 Mount Givens magma were 2-km thick, this would require only ~12 km^3 of mafic magma.

An examination of the Sierra Nevada batholith suggests that there is little potential for having remobilized significant volumes of magma via either of these mechanisms. Diorite and gabbro bodies are few in number relative to intermediate and felsic plutons (Fig. 7).

None appear to be large enough to rejuvenate a Mount Givens-sized crystal mush by gas sparging. Whereas the small mafic plutons that do exist may meet the volumetric requirements of unzipping, they do not have the lateral extent necessary to underplate the large areas of intermediate-composition intrusive suites found in the batholith. Even the deeper crystallization depths exposed in the southern Sierra Nevada batholith (Ague and Brimhall 1988) do not reveal the volumes or areas of mafic rocks thought to be necessary to cause the eruption of large-volume ash sheets, though it is possible that mafic bodies crystallizing at those depths may have sunk (Glazner and Miller 1997).

Furthermore, the rejuvenation hypotheses assume that the eventual eruption products were previously stored as long-lived mushes just above the solidus (e.g., Bachmann and Bergantz 2003; Bachmann et al. 2007; Huber et al. 2009; Burgisser and Bergantz 2011). However, modeling indicates that magmas intruded as sills at low accumulation rates will completely solidify before subsequent sills are emplaced (Annen 2009; Schöpa and Annen 2013). This is supported by thermochronologic data by Davis et al. (2012) that suggests magma in the John Muir Intrusive Suite cooled rapidly below hornblende Ar closure (~580-490°C) after emplacement (Fig. 8). Given the large span of zircon U-Pb ages presented here, it is likely that only small areas of the Mount Givens Granodiorite were melt-rich at any

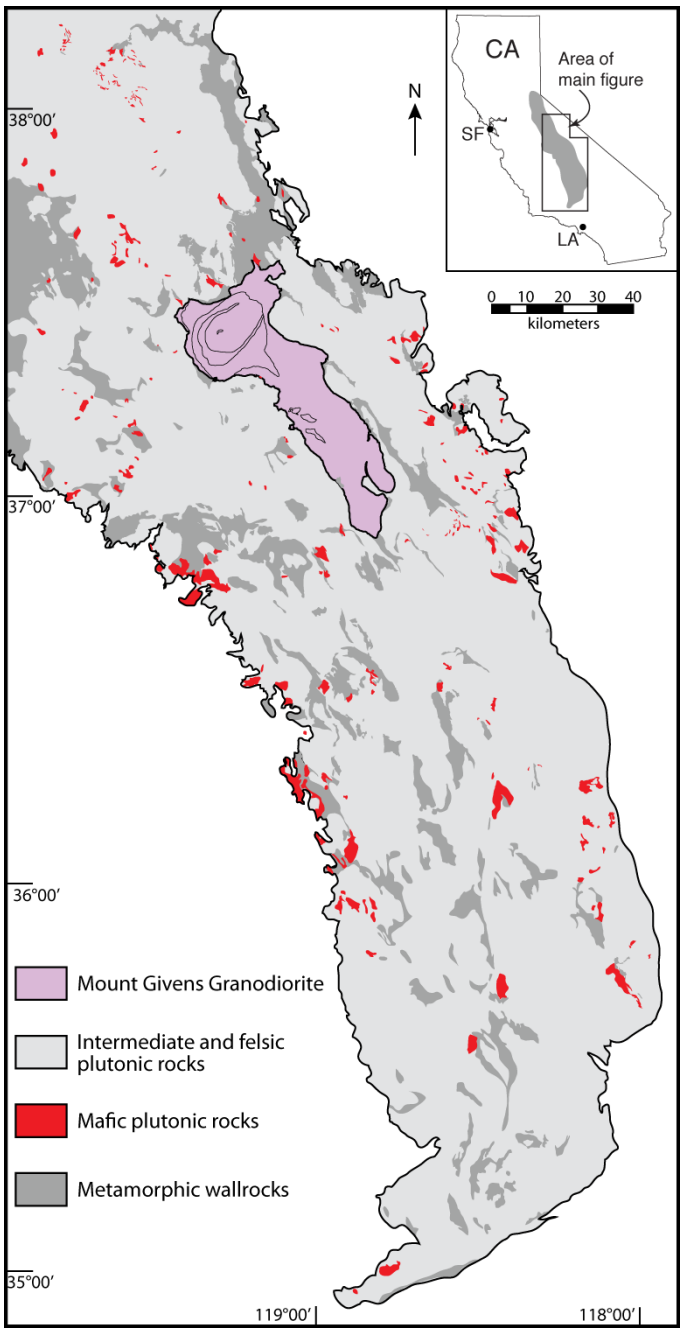

Figure 7. Generalized map of the central and southern Sierra Nevada batholith showing the distribution of mafic plutonic rocks relative to intermediate and felsic plutonic rocks. When highlighting mafic rocks, only gabbros and diorites were chosen if the maps specified them; otherwise the general categories "Mesozoic basic" and "Mesozoic ultrabasic" (e.g., Smith 1964) were highlighted. Rock types and locations after Moore (1963, 1978, 1981), Smith (1964), Matthews and Burnett (1965), Huber (1983), du Bray and Moore (1985), Moore and Sisson (1985, 1987), Diggles et al. (1987), Moore and Nokleberg (1992), Bateman (1992), Pickett and Saleeby (1993), Sisson and Moore (1994), Stone et al. (2000), Wahrhaftig (2000), and Lackey et al. (2008).

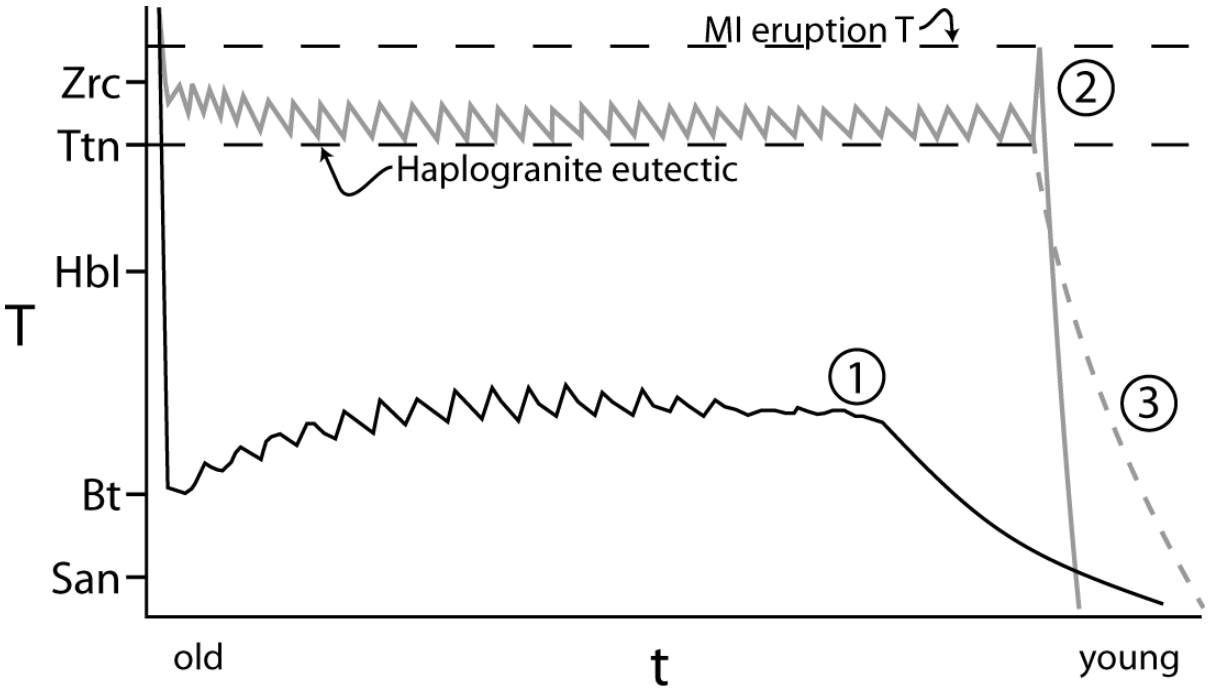

Figure 8. Schematic diagram indicating various T-t paths for intermediate magmas assuming incremental assembly of a large volume of magma. Relative closure temperatures of various thermochronometers are indicated on the y-axis; the temperature for zircon (Zrc) is a relative crystallization temperature. Ttn – titanite (U-Pb); Hbl – hornblende ($^{40}Ar/^{39}Ar$); Bt - biotite ($^{40}Ar/^{39}Ar$); San – sanidine (ignimbrites only; $^{40}Ar/^{39}Ar$). Path 1 indicates the T-t path of a small batch of magma that is emplaced as a sill in the upper crust. Paths 2 and 3 indicate the T-t paths that magmas follow according to the magma mush hypothesis, where eventual plutons and ignimbrites share most of the same T-t histories. In path 1, the magma rapidly solidifies then slowly increases in T as subsequent sills are emplaced. As the locus of magmatism retreats and eventually subsides, T decreases to background levels. This T-t path is in agreement with geothermochronology by Davis et al. (2012) that indicates synchronous zircon, titanite and hornblende ages, but biotite ages that are much younger. Paths 2 and 3 show the magma staying in a mushy state above the haplogranite eutectic for a long period of time after emplacement due to subsequent intrusions and latent heat buffering (Bachmann et al. 2007; Huber et al. 2009). The mush may then be rejuvenated and erupted as an MI (path 2) or heat input may cease entirely, allowing the mush to cool into a pluton (path 3). This would result in zircon ages that are significantly older than the closure dates from any of the thermochronometers, which has thus far not been observed in plutonic rocks.

given time during its emplacement. Thus, in order to cause a growing pluton similar to the Mount Givens Granodiorite to erupt such that it will result in a monotonous intermediate, volumes of underplating mafic magma even greater than those called upon by the rejuvenation hypotheses are required.

Pluton-volcano connections

The data presented here indicate that the difference in age spans between monotonous intermediates and plutons is related to different magma accumulation rates for the two. The information recorded by zircon in monotonous intermediates is indicative of high flux events that favor magma evacuation in large eruptions. These eruptions may leave little behind in the plutonic record, as evidenced by the lack of large volumes of cogenetic intrusive rocks with the tight age spans similar to those observed in ignimbrites (Tappa et al. 2011; Mills and Coleman 2013). Conversely, the lower fluxes observed in plutons are a reflection of the incremental emplacement of magmas that are preferentially stored in the crust, because they tend to cool rapidly after emplacement (Annen 2009; Davis et al. 2012; Schöpa and Annen 2013). Thus, whereas the Mount Givens Granodiorite's composition and volume are similar to those observed in large ignimbrites, it likely grew too slowly to support the formation of a volume of magma capable of supporting a "super-eruption".

Instead, I suggest that potential magma loss from the Mount Givens system would have resulted in typical arc stratovolcano activity. There are many similarities between pluton assembly rates and small-volume arc volcanic fluxes. For example, the average extrusion rate calculated for the Aucanquilcha volcanic center (0.00003 km^3/a; Grunder et al. 2006) is in fact slower than the construction rate of the Mount Givens pluton. In addition, Grunder et al. (2006) found that volcanism at the Aucanquilcha volcanic cluster progressed

from mafic to more felsic eruptive products over time, similar to that observed in large intrusive suites, and to a lesser extent, the Mount Givens Granodiorite.

VI. CONCLUSIONS

New high-precision U-Pb zircon data indicate that the Mount Givens Granodiorite was emplaced over a period of at least 7 Ma, from ~98-91 Ma. Previous growth models for the pluton, such as upper-crustal fractional crystallization (Bateman and Nokleberg 1978) or rapid emplacement of large sills (McNulty et al. 2000) do not satisfy the range of crystallization ages in the pluton. Instead, I suggest that the pluton was constructed incrementally by small batches of magma over time, as is observed in many other plutons and intrusive suites. Using the pluton's exposed area, relief and age range allows me to calculate a long-term average emplacement rate of 0.0006 km^3/a. This is similar to average rates found in other intrusive rocks, but is orders of magnitude slower than magma fluxes observed in large ignimbrites. Because the Mount Givens Granodiorite has been likened to monotonous intermediates, which are thought to erupt as the result of rejuvenating a slowly accumulated crystal mush, I investigated the effects of hypothetical reheating events on zircon that would be present in the system. I found that even under favorable conditions, it is difficult to dissolve zircon and thus it is likely that ignimbrites should preserve information about long-term magma accumulation if it occurred. The lack of multi-Ma age spans in zircons from monotonous intermediates, coupled with the presence of much older xenocrystic cores in some monotonous intermediates, suggests that monotonous intermediates are the result of high-flux events that preferentially end in voluminous eruptions. Conversely, low magma fluxes are conducive to accumulating and cooling small

batches of magma in the crust in the form of plutons. This activity may be reflected in the volcanic record by long-lived, small-volume volcanic fields.

APPENDIX 1

Cathodoluminescence images

Photomicrographs of zircon (Fig. 1) were collected using a TESCAN scanning electron microscope operating at 15 kV equipped with a cathodoluminescence detector. Images were collected on individual zircons. Contrast and brightness were adjusted for each image to improve visual clarity. Zircon images were cropped, rotated and placed on a black background. No images were collected for sample MG10-03 in order to preserve its sparse zircons for U-Pb geochronology.

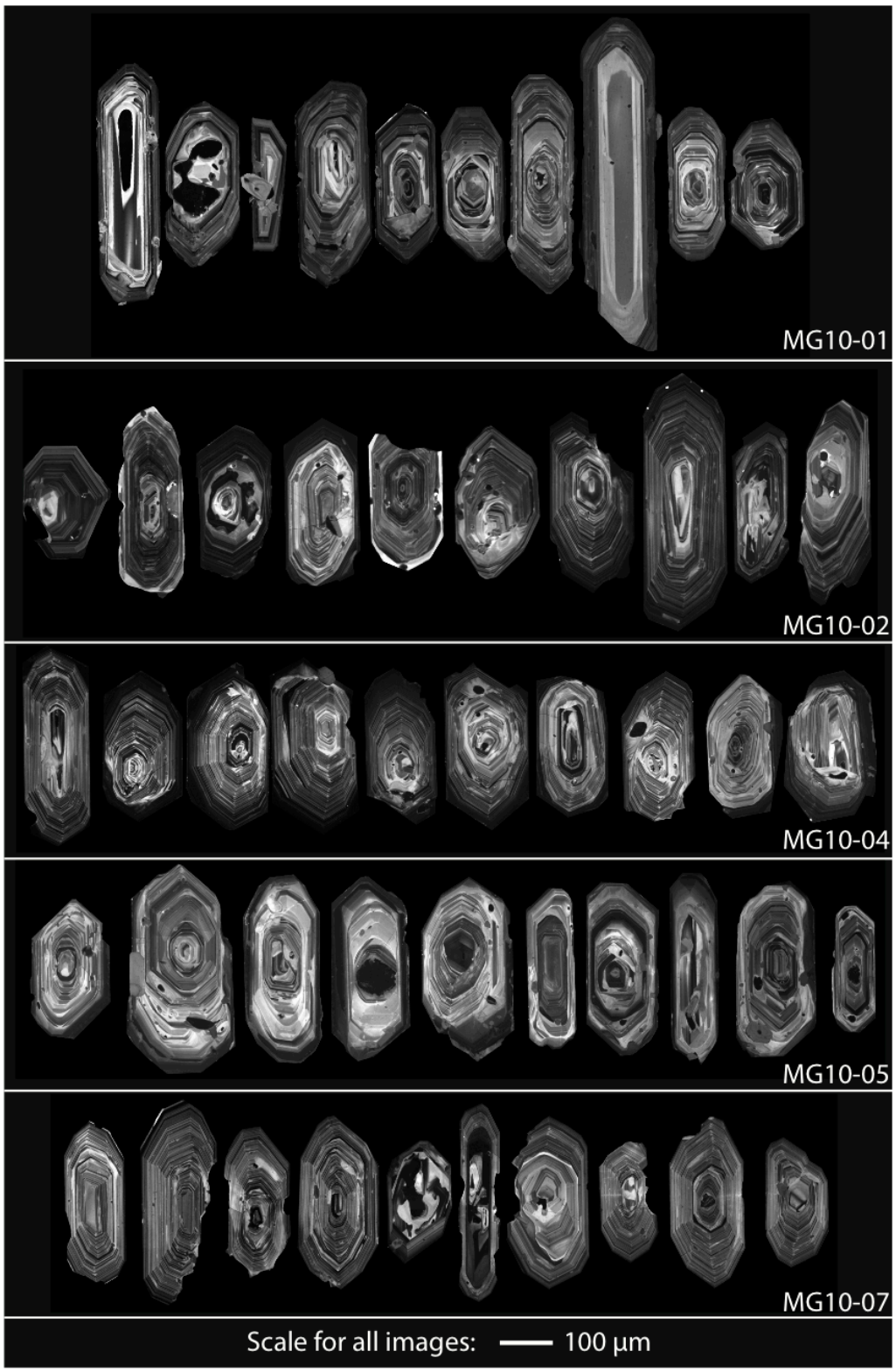

Figure 1. Cathodoluminescence images of typical zircon in samples dated from the Mount Givens Granodiorite. None of these specific zircons have been dated. Note that all zircons in all samples are shown at the same scale.

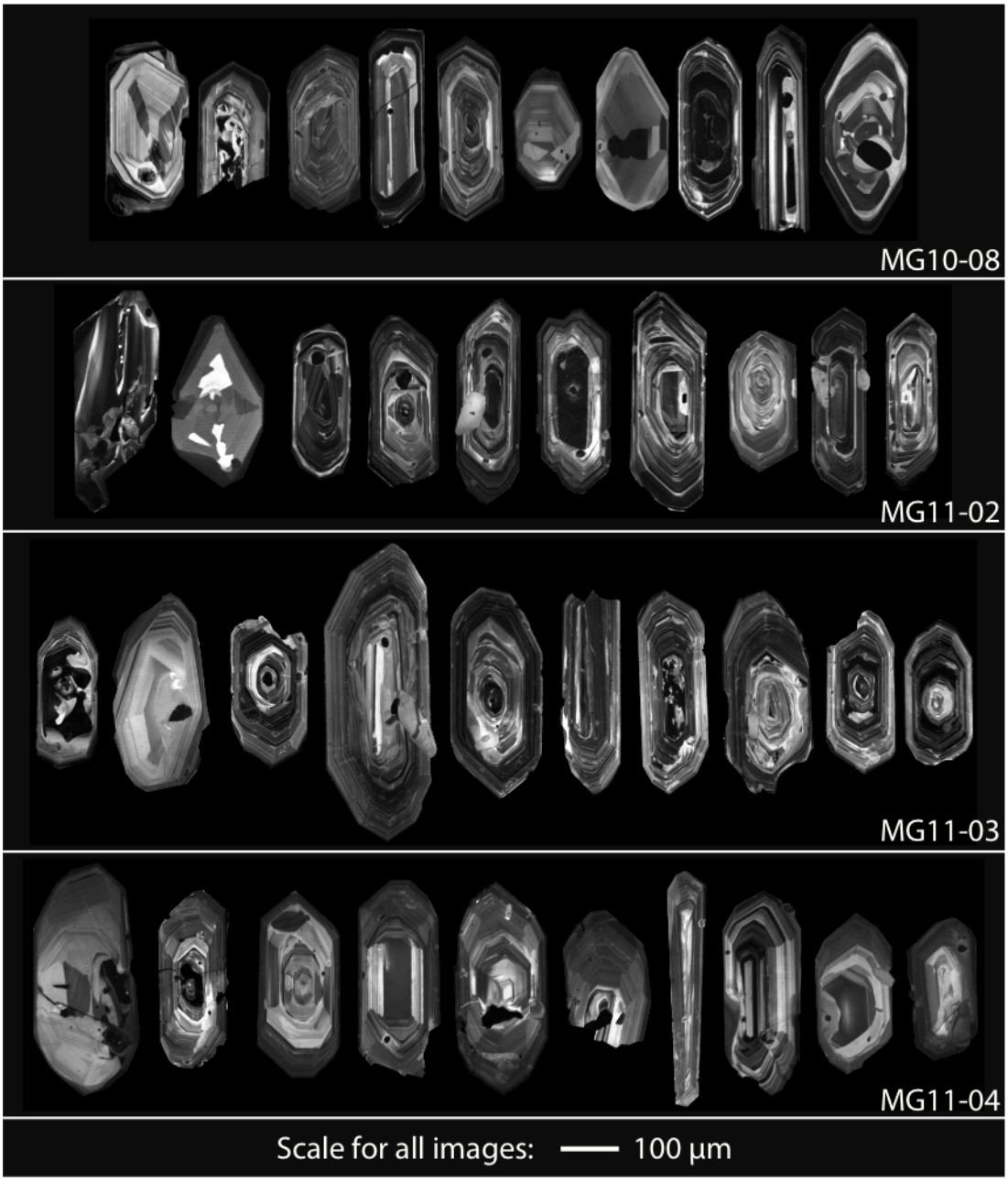

Figure 1 (cont.). Cathodoluminescence images of typical zircon in samples dated from the Mount Givens Granodiorite. None of these specific zircons have been dated. Note that all zircons in all samples are shown at the same scale.

APPENDIX 2

Zircon age data for rocks from the Mount Givens Granodiorite

sample fraction	U (ppm)	Pb[a] (pg)	Th[b] / U	^{206}Pb / ^{204}Pb[c]	^{206}Pb / ^{238}U[d]	error (%)	^{207}Pb / ^{235}U[d]	error (%)	^{207}Pb / ^{206}Pb[d]	error (%)	ages (Ma)[e] ^{206}Pb / ^{238}U	ages (Ma)[e] ^{207}Pb / ^{235}U	ages (Ma)[e] ^{207}Pb / ^{206}Pb	corr. coeff.	total[f] common Pb (pg)
MG10-01 Equigranular granodiorite (297825, 4153316)[g]															
F-1	925	131	0.40	2296	0.0149558	0.15	0.098896	0.54	0.047959	0.48	95.79	95.76	94.8	0.501	3.6
F-2	942	65	0.38	1280	0.0148744	0.12	0.098493	0.88	0.048025	0.83	95.28	95.38	98.1	0.526	3.3
F-4	814	120	0.42	6062	0.0149081	0.08	0.098783	0.26	0.048057	0.21	95.49	95.65	99.7	0.646	1.2
F-7	1075	56	0.35	4490	0.0148368	0.09	0.098342	0.33	0.048072	0.30	95.04	95.24	100.4	0.493	0.8
F-8	922	32	0.37	1613	0.0148255	0.13	0.098044	0.79	0.047964	0.73	94.97	94.97	95.0	0.540	1.3
F-13	317	32	0.39	721	0.0149286	0.14	0.100268	1.66	0.048713	1.57	95.62	97.02	131.6	0.631	2.8
MG10-02 Megacrystic granodiorite (299119, 4150174)															
F-1	470	31	0.38	946	0.0144093	0.14	0.095897	1.33	0.048268	1.23	92.32	92.98	110.0	0.702	2.1
F-5	553	42	0.39	915	0.0160345	0.22	0.107185	1.29	0.048482	1.21	102.64	103.39	120.6	0.429	3.0
F-6	1178	81	0.45	3459	0.0143706	0.14	0.094958	0.43	0.047924	0.37	92.07	92.11	93.1	0.566	1.5
F-9	243	52	0.43	1532	0.0147715	0.13	0.098209	0.78	0.048220	0.72	94.62	95.12	107.7	0.526	2.1
F-10	912	64	0.50	2077	0.0144672	0.10	0.095648	0.62	0.047950	0.57	92.69	92.75	94.4	0.583	1.9
F-11	1116	104	0.40	4437	0.0144432	0.09	0.095467	0.36	0.047939	0.31	92.54	92.58	93.8	0.641	1.5
F-14	957	86	0.48	2894	0.0150431	0.12	0.099769	0.46	0.048101	0.41	96.35	96.56	101.9	0.516	1.8
MG10-03 Aplitic granite (295531, 4144923)															
F-1	1039	63	0.45	686	0.0144594	0.14	0.095729	1.64	0.048017	1.55	92.64	92.83	97.7	0.662	5.9
F-2	2118	30	0.30	1302	0.0143416	0.12	0.094672	0.89	0.047876	0.83	91.89	91.85	90.6	0.540	1.5
F-3	2600	74	0.49	3068	0.0144802	0.12	0.095742	0.45	0.047954	0.39	92.77	92.84	94.6	0.580	1.5
F-4	801	34	0.48	2169	0.0144674	0.21	0.095616	0.83	0.047933	0.77	92.69	92.72	93.6	0.371	1.0
MG10-04 Megacrystic granodiorite (296797, 4145483)															
F-1	762	152	0.50	6423	0.0145414	0.09	0.096247	0.30	0.048004	0.24	93.16	93.31	97.1	0.736	1.5
F-3	1231	178	0.46	3985	0.0145218	0.09	0.095950	0.36	0.047921	0.31	93.03	93.03	92.9	0.594	2.8
F-5	118	33	0.46	2309	0.0144186	0.18	0.095680	0.63	0.048128	0.55	92.38	92.78	103.1	0.574	0.9
F-7	736	230	0.44	4572	0.0144520	0.10	0.095366	0.31	0.047859	0.26	92.59	92.49	89.9	0.615	3.2
MG10-05 Equigranular granodiorite (288528, 4136287)															
F-1	820	127	0.41	5359	0.0150757	0.10	0.099691	0.29	0.047960	0.23	96.55	96.49	94.9	0.654	1.5
F-2	260	95	0.43	3913	0.0150413	0.12	0.099474	0.35	0.047965	0.29	96.34	96.29	95.2	0.583	1.5

F-4	3342	143	0.42	5401	0.0150698	0.10	0.099826	0.31	0.048044	0.26	96.52	96.62	99.1	0.602	1.7
F-5	327	94	0.42	3896	0.0150844	0.11	0.100088	0.42	0.048123	0.38	96.61	96.86	103.0	0.508	1.5
F-6	486	67	0.36	3461	0.0150633	0.21	0.099793	0.41	0.048048	0.32	96.48	96.59	99.3	0.638	1.2
F-8	313	157	0.42	8078	0.0150331	0.12	0.099688	0.39	0.048094	0.29	96.28	96.49	101.5	0.872	1.2
MG10-07 Megacrystic granodiorite (326375, 4110337)															
F-1	633	105	0.63	4132	0.0140655	0.11	0.092879	0.43	0.047892	0.37	90.13	90.18	91.6	0.630	1.5
F-2	798	140	0.49	5744	0.0142032	0.11	0.093807	0.32	0.047901	0.26	91.01	91.04	91.9	0.662	1.5
F-3	696	179	0.51	6079	0.0141686	0.10	0.093480	0.33	0.047851	0.30	90.79	90.74	89.5	0.361	1.8
F-4	676	106	0.53	4422	0.0141932	0.14	0.093838	0.35	0.047951	0.29	90.94	91.07	94.4	0.617	1.5
F-7	475	94	0.68	4624	0.0141685	0.11	0.093480	0.32	0.047851	0.27	90.78	90.74	89.6	0.615	1.2
F-8	448	106	0.54	2761	0.0141954	0.32	0.093637	0.53	0.047841	0.39	90.96	90.89	89.0	0.676	2.3
MG10-08 Aplitic granite (324733, 4113647)															
F-1	214	69	0.50	3171	0.0144533	0.11	0.095382	0.53	0.047863	0.47	92.60	92.50	90.1	0.646	1.3
F-2	870	58	0.69	2441	0.0142017	0.12	0.093864	0.53	0.047935	0.48	90.99	91.10	93.8	0.511	1.4
F-4	639	99	0.44	2952	0.0144307	0.10	0.094960	0.51	0.047726	0.46	92.46	92.11	83.3	0.596	2.1
F-5	798	131	0.54	2364	0.0142049	0.11	0.093700	0.51	0.047841	0.46	91.02	90.94	89.0	0.516	3.4
MG11-02 Megacrystic granodiorite (312408, 4132076)															
F-3	902	121	0.45	6119	0.0149241	0.17	0.098947	0.36	0.048086	0.28	95.59	95.80	101.1	0.646	1.2
F-4	434	84	0.44	3127	0.0149194	0.13	0.098739	0.44	0.048000	0.38	95.56	95.61	96.9	0.559	1.7
MG11-03 Equigranular granodiorite (290404, 4140734)															
F-1	745	303	0.48	10007	0.0148615	0.08	0.097926	0.20	0.047790	0.14	95.19	94.86	86.5	0.809	1.9
F-3	874	374	0.38	10047	0.0147955	0.08	0.097332	0.20	0.047712	0.14	94.78	94.31	82.6	0.765	2.4
F-4	748	102	0.38	4655	0.0147705	0.09	0.097329	0.29	0.047791	0.24	94.62	94.31	86.5	0.639	1.4
F-10	742	64	0.40	909	0.0147417	0.12	0.097653	1.22	0.048044	1.16	94.43	94.61	99.0	0.581	4.5
MG11-04 Megacrystic granodiorite (283917, 4149984)															
F-1	148	62	0.45	2107	0.0152823	0.10	0.101211	0.57	0.048033	0.52	97.87	97.89	98.6	0.521	1.8
F-3	570	107	0.46	2657	0.0152846	0.18	0.101111	0.48	0.047978	0.41	97.88	97.80	95.9	0.537	2.5
F-4	380	80	0.48	4339	0.0153922	0.09	0.101809	0.31	0.047972	0.26	98.56	98.44	95.6	0.636	1.1

[a] Total mass of radiogenic Pb

[b] Th contents calculated from radiogenic ^{208}Pb and the $^{207}Pb/^{206}Pb$ date of the sample, assuming concordance between U-Th and Pb systems

[c] Measured ratio corrected for fractionation and spike contribution only

[d] Measured ratios corrected for fractionation, tracer, blank

[e] Th-corrected isotopic dates calculated using the decay constants $\lambda_{238} = 1.55125E^{-10}$ and $\lambda_{235} = 9.8485E^{-10}$ (Jaffey et al. 1971), assuming $Th/U_{magma} = 3.7$

[f] Total mass of common Pb

[g] Locations in NAD 83, UTM Zone 11

APPENDIX 3

Modeling mafic magma volumes required for rejuvenation of the Mount Givens Granodiorite

The amount of mafic magma necessary to rejuvenate the Mount Givens Granodiorite is calculated using the "gas sparging" method (Bachmann and Bergantz 2003, 2006; Huber et al. 2010). In the "gas sparging" hypothesis, basaltic magma underplates a locked silicic magma mush (50+% crystals; Bachmann and Bergantz 2006). As the basalt crystallizes, it releases volatiles (H_2O+CO_2), which may advect heat into the overlying silicic mush without leaving an easily detectable chemical signature (Bachmann and Bergantz 2003, 2006). This may cause resorption of crystals in the locked mush, allowing it to convect and homogenize.

The volume of mafic magma may be determined by equating the amount of energy required to raise the temperature of the silicic mush and melt a fraction of the crystals in the mush with the amount of sensible and latent heat released by the crystallizing mafic magma (Bachmann and Bergantz 2003, 2006), while also accounting for conductive cooling of the mush over the time period in question. This is represented in the following equation

$$m_{\text{mafic}} = \frac{\{m_{\text{mush}}[C_{p,\text{mush}}\Delta T_{\text{mush}} + X_m L_{\text{mush}}]\} + (-k)A\dfrac{\Delta T_{\text{mush}}}{\Delta x}\Delta t}{C_{p,\text{mafic}}\Delta T_{\text{mafic}} + X_c L_{\text{mafic}}}$$

All parameters are defined in Table 1 and were taken from Bachmann and Bergantz (2003, 2006) where applicable. Bachmann and Bergantz (2003, 2006) used an integrated form of Fourier's law assuming a depth between 6 and 7 km for the top of the magma chamber (Δx) to calculate the amount of heat lost by conductive cooling over 150 ka (O Bachmann pers. comm.). The mass of the Mount Givens crystal mush was calculated assuming a volume of 4500 km^3 and a density of 2450 kg m^{-3}, whereas the final volume of the mafic magma was calculated assuming a density of 2900 kg m^{-3} (Bachmann and Bergantz 2003, 2006).

Table 1. Parameters used in gas sparging calculations

Symbol	Definition	Value	Source[a]
m_{mush}	Mass of the mush (kg)	1.1025×10^{16}	this study
m_{mafic}	Mass of mafic magma (kg)		
$C_{p,\text{mush}}$	Specific heat, mush (J kg^{-1} K^{-1})	1370	B and B 2003
$C_{p,\text{mafic}}$	Specific heat, mafic magma (J kg^{-1} K^{-1})	1484	B and B 2003
ΔT_{mush}	$T_{initial} - T_{final,}$ in mush (K)	40	B and B 2003
ΔT_{mafic}	$T_{initial} - T_{final,}$ in mafic magma (K)	150	B and B 2003
X_m	Weight fraction melted, mush	0.2	B and B 2003
X_c	Weight fraction crystallized, mafic magma	0.9	B and B 2003
L_{mush}	Latent heat of fusion, mush (J kg^{-1})	2.7×10^5	B and B 2003
L_{mafic}	Latent heat of fusion, mafic magma (J kg^{-1})	4×10^5	B and B 2003
k	Thermal conductivity (W m^{-1} K^{-1})	2	B and B 2006
A	Cross-sectional area (m^2)	1.5×10^9	B and B 2003
Δx	Distance between ends (m)	1000	OB pers. comm. 2010
Δt	Time elapsed (s)	4.73×10^{12}	B and B 2003

[a]B and B: Bachmann and Bergantz; OB: O. Bachmann

REFERENCES

Ague JJ, Brimhall GH (1988) Magmatic arc asymmetry and distribution of anomalous plutonic belts in the batholiths of California: Effects of assimilation, crustal thickness, and depth of crystallization. Geol Soc Am Bull 100:912-927

Annen C (2009) From plutons to magma chambers: Thermal constraints on the accumulation of eruptible silicic magma in the upper crust. Earth Planet Sci Lett 284:409-416

Annen C, Blundy JD, Sparks RSJ (2006) The Genesis of Intermediate and Silicic Magmas in Deep Crustal Hot Zones. J Petrol 37:505-539

Bachmann O (2010) The petrologic evolution and pre-eruptive conditions of the rhyolitic Kos Plateau Tuff (Aegean arc). Cent Eur J Geosci 2:270-305

Bachmann O, Dungan MA (2002) Temperature-induced Al-zoning in hornblendes of the Fish Canyon magma. Am Mineral 87:1062-1076

Bachmann O, Bergantz GW (2003) Rejuvenation of the Fish Canyon magma body: A window into the evolution of large-volume silicic magma systems. Geology 31:789-792

Bachmann O, Bergantz GW (2006) Gas percolation in upper-crustal silicic crystal mushes as a mechanism for upward heat advection and rejuvenation of near-solidus magma bodies. J Volcanol Geotherm Res 149:85-102

Bachmann O, Bergantz GW (2008) Rhyolites and their Source Mushes across Tectonic Settings. J Petrol 49:2277-2285

Bachmann O, Dungan MA, Lipman PW (2002) The Fish Canyon Magma Body, San Juan Volcanic Field, Colorado: Rejuvenation and Eruption of an Upper-Crustal Batholith. J Petrol 43:1469-1503

Bachmann O, Miller CF, de Silva SL (2007) The volcanic-plutonic connection as a stage for understanding crustal magmatism. J Volcanol Geotherm Res 167:1-23

Bateman PC (1965) Geologic map of the Blackcap Mountain quadrangle, Fresno County, California. US Geol Surv Rep GQ-428

Bateman PC (1992) Plutonism in the Central Part of the Sierra Nevada Batholith, California. US Geol Surv Prof Pap 1483

Bateman PC, Nokleberg WJ (1978) Solidifcation of the Mount Givens Granodiorite, Sierra Nevada, California. J Geology 86:563-579

Bateman PC, Chappell BW (1979) Crystallization, fractionation, and solidification of the Tuolumne Intrusive Series, Yosemite National Park, California. Geol Soc Am Bull 90:465-482

Bateman PC, Lockwood JP, Lydon PA (1971) Geologic map of the Kaiser Peak quadrangle, central Sierra Nevada, California. US Geol Surv Rep GQ-894

Bindeman IN (2003) Crystal sizes in evolving silicic magma chambers. Geology 31:367-370

Bowring JF, McLean NM, Bowring SA (2011) Engineering cyber infrastructure for U-Pb geochronology: Tripoli and U-Pb_Redux. Geochem Geophys Geosyst, 12:Q0AA19. doi:10.1029/2010GC003479

Burgisser A, Bergantz GW (2011) A rapid mechanism to remobilize and homogenize highly crystalline magma bodies. Nature 471:212-215

Chesner CA (1998) Petrogenesis of the Toba Tuffs, Sumatra, Indonesia. J Petrol 39:397-438

Chesner CA (2011) The Toba Caldera Complex. Quat Int 258:5-18

Coleman DS, Gray W, Glazner AF (2004) Rethinking the emplacement and evolution of zoned plutons: Geochronologic evidence for incremental assembly of the Tuolumne Intrusive Suite, California. Geology 32:433-436

Couch S, Sparks RSJ, Carroll MR (2001) Mineral disequilibrium in lavas explained by convective self-mixing in open magma chambers. Nature 411:1037-1039

Corfu F, Hanchar JM, Hoskin PWO, Kinny P. (2003) Atlas of zircon textures. In: Hanchar JM, Hoskin PWO (eds) Zircon. Rev Mineral Geochem 53:468-500

Crisp JA (1984) Rates of magma emplacement and volcanic output. J Volc Geotherm Res 20:177-211

Crowley JL, Schoene B, Bowring SA (2007) U-Pb dating of zircon in the Bishop Tuff at the millennial scale. Geology 35:1123-1126

Cruden AR (1998) On the emplacement of tabular granites. J Geol Soc Lond 155:853-862

Cruden AR, Launeau P (1994) Structure, magnetic fabric and emplacement of the Archean Lebel Stock, SW Abitibi Greenstone Belt. J Struct Geol 16:677-691

Cruden AR, Tobisch OT, Launeau P (1999) Magnetic fabric evidence for conduit-fed emplacement of a tabular intrusion: Dinkey Creek Pluton, central Sierra Nevada batholith, California. J Geophys Res 104:10511-10530

Davis JW, Coleman DS (2008) Thermal models of incremental pluton emplacement. Geochim Cosmochim Acta 72:A202

Davis JW (2010) Thermochronology and cooling histories of plutons: implications for incremental pluton assembly. Dissertation, University of North Carolina at Chapel Hill

Davis JW, Coleman DS, Gracely JT, Gaschnig R, Stearns M (2012) Magma accumulation rates and thermal histories of plutons of the Sierra Nevada batholith, CA. Contrib Mineral Petrol 163:449-465

de Saint Blanquat M, Tikoff B (1997) Development of magmatic to solid-state fabrics during syntectonic emplacement of the Mono Creek granite, Sierra Nevada batholith. In: Bouchez JL, Hutton DHW, Stephens WE (eds) Granite: From segregation of melt to emplacement fabrics. Kluwer Academic Publishers, Amsterdam, pp 231–252

de Saint Blanquat M, Horsman E, Habert G, Morgan S, Vanderhaeghe O, Law R, Tikoff B (2011) Multiscale magmatic cyclicity, duration of pluton construction, and the paradoxical relationship between tectonism and plutonism in continental arcs. Tectonophysics 500:20-33

de Silva SL, Gosnold WD (2007) Episodic construction of batholiths: Insights from the spatiotemporal development of an ignimbrite flare-up. J Volc Geotherm Res 167:320-335

Diggles MF, Dellinger DA, Conrad JE (1987) Geologic map of the Owens Peak and Little Lake Canyon Wilderness study areas, Inyo and Kern Counties, California. US Geol Surv Rep MF-1927-A

Dodge FCW, Millard HT Jr, Elsheimer HN (1982) Compositional Variations and Abundances of Selected Elements in Granitoid Rocks and Constituent Minerals, Central Sierra Nevada Batholith, California. US Geol Surv Prof Pap 1248

du Bray EA, Moore JG (1985) Geologic map of the Olancha quadrangle, southern Sierra Nevada, California. US Geol Surv Rep MF-1734

Frazer RE, Lackey JS, Valencia VA (2009) New U-Pb zircon ages of the granites of Dinkey Dome: Reexamining the origins of the Shaver Intrusive Suite. Geol Soc Am Abs Prog 41:14

Gilder S, McNulty BA (1999) Tectonic exhumation and tilting of the Mount Givens pluton, central Sierra Nevada, California. Geology 27:919-922

Glazner AF, Miller DM (1997) Late-stage sinking of plutons. Geology 25:1099-1102

Glazner AF, Bartley JM, Coleman DS, Gray W, Taylor RZ (2004) Are plutons assembled over millions of years by amalgamation from small magma chambers? Geol Soc Am Today 14:4-11

Grunder AL, Klemetti EW, Feeley TC, McKee CM (2006) Eleven million years of arc volcanism at the Aucanquilcha Volcanic Cluster, northern Chilean Andes: implications for the life span and emplacement of plutons. Trans R Soc Edinb Earth Sci 97:415-436

Guillet P, Bouchez JL, Wagner JJ (1983) Anisotropy of magnetic susceptibility and magmatic structures in the Guérande granite massif (France). Tectonics 2:419-429

Hamilton W, Myers WB (1967) The Nature of Batholiths. US Geol Surv Prof Pap 554-C

Hildreth W (1981) Gradients in Silicic Magma Chambers: Implications for Lithospheric Magmatism. J Geophys Res 86:10153-10192

Hildreth W (2004) Volcanological perspectives on Long Valley, Mammoth Mountain, and Mono Craters: several contiguous but discrete systems. J Volc Geotherm Res 136:169-198

Huber C, Bachmann O, Manga M, (2009) Homogenization processes in silicic magma chambers by stirring and mushification (latent heat buffering). Earth Planet Sci Lett 283:38-47

Huber C, Bachmann O, Manga M (2010) Two Competing Effects of Volatiles on Heat Transfer in Crystal-rich Magmas: Thermal Insulation vs. Defrosting. J Petrol 51:847-867

Huber C, Bachmann O, Dufek J (2012) Crystal-poor versus crystal-rich ignimbrites: A competition between stirring and reactivation. Geology 40:115-118

Huber NK (1983) Preliminary geologic map of the Pinecrest quadrangle, central Sierra Nevada, California. US Geol Surv Rep MF-1437

Huang F, Lundstrom CC, Glessner J, Ianno A, Boudreau A, Li J, Ferré EC, Marshak S, DeFrates J (2009) Chemical and isotopic fractionation of wet andesite in a temperature gradient: Experients and models suggesting a new mechanism of magma differentiation. Geochim Cosmochim Acta 73:729-749

Johnson BR, Glazner AF (2010) Formation of K-feldspar megacrysts in granodioritic plutons by thermal cycling and late-stage textural coarsening. Contrib Mineral Petrol 159:599-619

King RF (1966) The magnetic susceptibility of some Irish granites. Geol J 5:43-66

Krogh TE (1973) A low-contamination method for hydrothermal decomposition of zircon and extraction of U and Pb for isotopic age determinations. Geochim Cosmochim Acta 37:485-494

Lackey JS, Valley JW, Chen JH, Stockli DF (2008) Dynamic Magma Systems, Crustal Recycling, and Alteration in the Central Sierra Nevada. J Petrol 49:1397-1426

Lackey JS, Cecil MR, Windham CJ, Frazer RE, Bindeman IN, Gehrels GE (2012) The Fine Gold Intrusive Suite: The roles of basement terranes and magma source development in the Early Cretaceous Sierra Nevada Batholith. Geoshpere 8:292-313

Lanphere MA, Baadsgaard H (2001) Precise K–Ar, $^{40}Ar/^{39}Ar$, Rb–Sr and U/Pb mineral ages from the 27.5 Ma Fish Canyon Tuff reference standard. Chem Geol 175:653-671

Leuthold J, Müntener O, Baumgartner LP, Putlitz B, Ovtcharova M, Schaltegger U (2012) Time resolved construction of a bimodal laccolith (Torres del Paine, Patagonia). Earth Planet Sci Lett 325-326:85-92

Lindsay JM, de Silva S, Trumbull R, Emmermann R, Wemmer K (2001a) La Pacana caldera, N. Chile: a re-evaluation of the stratigraphy and volcanology of one of the world's largest resurgent calderas. J Volc Geotherm Res 106:145-173

Lindsay JM, Schmitt AK, Trumbull RB, de Silva SL, Siebel W, Emmermann R (2001b) Magmatic Evolution of the La Pacana Caldera System, Central Andes, Chile: Compositional Variation of Two Cogenetic, Large-Volume Felsic Ignimbrites. J Petrol 42:459-486

Lipman PW (2007) Incremental assembly and prolonged consolidation of Cordilleran magma chambers: Evidence from the Southern Rocky Mountain volcanic field. Geoshpere 3:42-70

Lundstrom C (2009) Hypothesis for the origin of convergent margin granitoids and Earth's continental crust by thermal migration zone refining. Geochim Cosmochim Acta 73:5709-5729

Lundstrom CC, Marshak S, DeFrates J, Mabon J (2011) Alternative processes for developing fabric and mineral compositional zoning in intrusive rocks. Int Geol Rev 53:377-405

Mahood GA (1990) Second reply to comment of R.S.J. Sparks, H.E. Huppert and C.J.N. Wilson on "Evidence for long residence times of rhyolitic magma in the Long Valley magmatic system: the isotopic record in the precaldera lavas of Glass Mountain". Earth Planet Sci Lett 99:395-399

Matthews RA, Burnett JL (1965) Geologic map of California, Fresno sheet. State Calif Dep Conserv Div Mines Geol

Mattinson JM (2005) Zircon U-Pb chemical abrasion ("CA-TIMS") method: Combined annealing and multi-step partial dissolution analysis for imporved precision and accuracy of zircon ages. Chem Geol 220:47-66

Matzel JEP, Bowring SA, Miller RB (2006) Time scales of pluton construction at differing crustal levels: Examples from the Mount Stuart and Tenpeak intrusions, North Cascades, Washington. Geol Soc Am Bull 118:1412-1430

Maughan LL, Christiansen EH, Best MG, Grommé CS, Deino AL, Tingey DG (2002) The Oligocene Lund Tuff, Great Basin, USA: a very large volume monotonous intermediate. J Volc Geotherm Res 113:129-157

McLean NM, Bowring JF, Bowring SA, (2011) An algorithm for U-Pb isotope dilution data reduction and uncertainty propagation. Geochem Geophys Geosyst, 12:Q0AA18, doi:10.1029/2010GC003478.

McNulty BA, Tobisch OR, Cruden AR, Gilder S (2000) Multistage emplacement of the Mount Givens pluton, central Sierra Nevada batholith, California. Geol Soc Am Bull 112:119-135

Memeti V, Paterson S, Matzel J, Mundil R, Okaya D (2010) Magmatic lobes as "snapshots" of magma chamber growth and evolution in large, composite batholiths: An example from the Tuolumne intrusion, Sierra Nevada, California. Geol Soc Am Bull 122:1912-1931

Menand T (2011) Physical controls and depth of emplacement of igneous bodies: A review. Tectonophysics 500:11-19

Miller JS, Matzel JEP, Miller CF, Burgess SD, Miller RB (2007) Zircon growth and recycling during the assembly of large, composite arc plutons. J Volc Geotherm Res 167:282-299

Mills RD, Coleman DS (2013) Temporal and chemical connections between plutons and ignimbrites from the Mount Princeton magmatic center. Contrib Mineral Petrol, doi: 10.1007/s00410-012-0843-4

Mills RD, Ratner JJ, Glazner AF (2011) Experimental evidence for crystal coarsening and fabric development during temperature cycling. Geology 39:1139-1142

Molloy C, Shane P, Nairn I (2008) Pre-eruption thermal rejuvenation and stirring of a partly crystalline rhyolite pluton revealed by the Earthquake Flat Pyroclastics deposits, New Zealand. J Geol Soc 165:435-447

Moore JG (1963) Geologic map and sections of the Mount Pinchot quadrangle, California. US Geol Surv Bull 1130

Moore JG (1978) Geologic map of the Marion Peak quadrangle, Fresno County, California. US Geol Surv Rep GQ-1399

Moore JG (1981) Geologic map of the Mount Whitney quadrangle, Inyo and Tulare Counties, California. US Geol Surv Rep GQ-1545

Moore JG, Nokleberg WJ (1992) Geologic map of the Tehipite Dome quadrangle, Fresno County, California. US Geol Surv Rep GQ-1676

Moore JG, Sisson TW (1985) Geologic map of the Kern Peak quadrangle, Tulare County, California. US Geol Surv Rep GQ-1584

Moore JG, Sisson TW (1987) Geologic map of the Triple Divide Peak quadrangle, Tulare County, California. US Geol Surv Rep GQ-1636

Noyes HJ, Frey FA, Wones DR (1983) A Tale of Two Plutons: Geochemical Evidence Bearing on the Origin and Differentiation of the Red Lake and Eagle Peak Plutons, Central Sierra Nevada, California. J Geol 91:487-509

Parrish RR (1987) An improved micro-capsule for zircon dissolution in U-Pb geochronology. Chem Geol 66:99-102

Parrish RR, Krogh TE (1987) Synthesis and purification of ^{205}Pb for U-Pb geochronology. Chem Geol 66:103-110

Petford N, Cruden AR, McCaffrey KJW, Vigneresse JL (2000) Granite magma formation, transport and emplacement in the Earth's crust. Nature 408:669-673

Pickett DA, Saleeby JB (1993) Thermobarometric Constraints on the Depth of Exposure and Conditions of Plutonism and Metamorphism at Deep Levels of the Sierra Nevada Batholith, Tehachapi Mountains, California. J Geophys Res 98:609-629

Renne PR, Tobisch OT, Saleeby JB (1993) Thermochronologic record of pluton emplacement, deformation, and exhumation at Courtright shear zone, central Sierra Nevada, California. Geology 21:331-334

Rioux M, Lissenberg CJ, McLean NM, Bowring SA, MacLeod CJ, Hellebrand E, Shimizu N (2012) Protracted timescales of lower crustal growth at the fast-spreading East Pacific Rise. Nat Geosci 5:275-278

Schaltegger U, Brack P, Ovtcharova M, Peytcheva I, Schoene B, Stracke A, Marocchi M, Bargossi GM (2009) Zircon and titanite recording 1.5 million years of magma accretion, crystallization and initial cooling in a composite pluton (southern Adamello batholith, northern Italy). Earth Planet Sci Lett 286:208-218

Schmitt AK, Lindsay JM, de Silva S, Trumbull RB (2002) U-Pb zircon chronostratigraphy of early-Pliocene ignimbrites from La Pacana, north Chile: implications for the formation of stratified magma chambers. J Volc Geotherm Res, 120:43-53

Schmitz MD, Bowring SA (2001) U-Pb zircon and titanite systematics of the Fish Canyon Tuff: an assessment of high-precision U-Pb geochronology and its application to young volcanic rocks. Geochim Cosmochim Acta 65:2571-2587

Schmitz MD, Schoene B (2007) Derivation of isotope ratios, errors, and error correlations for U-Pb geochronology using ^{205}Pb-^{235}U-(^{233}U)-spiked isotope dilution thermal ionization mass spectrometric data. Geochem Geophys Geosyst 8:Q08006, doi:10.1029/2006GC001492

Schoene B, Latkoczy C, Schaltegger U, Günther D (2010) A new method integrating high-precision U–Pb geochronology with zircon trace element analysis (U–Pb TIMS-TEA). Geochim Cosmochim Acta 74:7144-7159

Schöpa A, Annen C (2013) The effects of magma flux variations on the formation and lifetime of large silicic magma chambers. J Geophys Res, doi:10.1002/jgrb.50127

Shane P, Nairn IA, Smith VC, Darragh M, Beggs K, Cole JW (2008) Silicic recharge of multiple rhyolite magmas by basaltic intrusion during the 22.6 ka Okareka Eruption Episode, New Zealand. Lithos 103:527-549

Sisson TW, Moore JG (1994) Geologic map of the Giant Forest quadrangle, Tulare County, California. US Geol Surv Rep GQ-1751

Smith AR (1964) Geologic map of California, Bakersfield sheet. State Calif Dep Conserv Div Mines Geol

Steiger RH, Jäger E (1977) Subcommission on geochronology: Convention on the use of decay constants in geo- and cosmochronology. Earth Planet Sci Lett 36:359-362

Stern TW, Bateman PC, Morgan BA, Newell MF, Peck DL (1981) Isotopic U-Pb ages of Zircon from the Granitoids of the Central Sierra Nevada, California. US Geol Surv Prof Pap 1185

Stone P, Dunne GC, Moore JG, Smith GI (2000) Geologic map of the Lone Pine 15' quadrangle, Inyo County, California. US Geol Surv Rep I-2617

Tappa MJ, Coleman DS, Mills RD, Samperton KM (2011) The plutonic record of a silicic ignimbrite from the Latir volcanic field, New Mexico. Geochem Geophys Geosyst 12:Q10011, doi: 10.1029/2011gc003700.

Tikoff B, de Saint Blanquat M (1997) Transpressional shearing and strike-slip partitioning in the Late Cretaceous Sierra Nevada magmatic arc, California. Tectonics 16:442-459

Tikoff B, Davis MR, Teyssier C, de Saint Blanquat M, Habert G, Morgan S (2005) Fabric studies within the Cascade Lake shear zone, Sierra Nevada, California. Tectonophysics 400:209-226

Tobisch OT, Renne PR, Saleeby JB (1993) Deformation resulting from regional extension during pluton ascent and emplacement, central Sierra Nevada, California. J Struct Geol 15:609-628

Tobisch OT, Saleeby JB, Renne PR, McNulty B, Tong W (1995) Variations in deformation fields during development of a large-volume magmatic arc, central Sierra Nevada, California. Geol Soc Am Bull 107:148-166

Vazquez JA, Reid MR (2004) Probing the Accumulation History of the Voluminous Toba Magma. Science 305:991-994

Wahrhaftig C (2000) Geologic map of the Tower Peak quadrangle, central Sierra Nevada, California. US Geol Surv Rep I-2697

Wark DA, Hildreth W, Spear FS, Cherniak DJ, Watson EB (2007) Pre-eruption recharge of the Bishop magma system. Geology 35:235-238

Watson EB (1996) Dissolution, growth and survival of zircons during crustal fusion: kinetic principles, geological models and implications for isotopic inheritance. Trans R Soc Edinb Earth Sci 87:43-56

Zimmerer MJ, McIntosh WC (2012) The geochronology of volcanic and plutonic rocks at the Questa caldera: Constraints on the origin of caldera-related silicic magmas. Geol Soc Am Bull 124:1394-1408